CHAPTER VII

FLOW INDUCED MOTION OF TWO CYLINDERS IN TANDEM

In Part A of this dissertation, FIM of multiple-cylinders has been studied extensively with variable spacing, position of PTC, and number of cylinders. In all tests with PTC, all cylinders achieved back-to-back VIV and galloping. Cylinder oscillatory amplitude reached up to $2.2-2.9D$, which was the maximum achievable amplitude experimentally due to the free-surface and the safety-stops which limited the travel. Ding et al. (2013) studied FIM of two rigid circular cylinders in tandem which were free to oscillate transversely to the flow by using two-dimensional Unsteady Reynolds-Averaged Navier-Stokes simulation. The simulation results are in excellent agreement with the experimental data presented in this dissertation and show that the oscillatory amplitude in galloping can reach up to $3.5D$ which is beyond the achievable amplitude with the old Low Turbulence Free Surface Water (LTFSW) Channel in the MRELab. The new VIVACE converters in the new LTFSW Channel, however, can achieve an oscillation amplitude up to $6D$ and thereby we can investigate the response of the cylinder in galloping further. FIM of two-cylinders with surface roughness (PTC) for high Re has been studied only by the MRELab to the best of the authors' knowledge (Kim et al., 2011). In this chapter, FIM of two cylinders is studied further in the range of 23,600<Re<104,200, which falls in the high-lift

TrSL3 regime. The spacing between the cylinder centers varies from $1.43D$ to $4.0D$ whereas the spacing of *2D* was the closest experimental setup in Part A. Moreover, effects of the spring stiffness and mass ratio on FIM are investigated, which were not considered as parameters in the tests in Part A.

7.1 Apparatus

7.1.1 New Low Turbulence Free Surface Water Channel

The LTFSW Channel was replaced by the new LTFSW Channel as shown in Figure 6.1 in May, 2012. The new channel recirculates about 38,000 liters of fresh water at speed up to 1.5m/s by an impeller powered by a 20hp induction motor and enables a continuous flow of water through the test section. In Chapter 6, the measurement results of the velocity distributions of the test section flow were presented and indirect methods to determine the mean velocity were proposed. The test section is made of plexiglass and is 2.44m long, 1m wide, and 1.542m deep. All tests presented in this chapter were conducted in the new LTFSW Channel using the newly built oscillators

7.1.2 Instrumentation and data collection

The cylinder oscillatory displacement is measured by a cable extension position transducer. The displacement data is measured for 60 seconds after the flow in the test section reaches steady state. For amplitude plots, the RMS of the 60 largest (positive and negative) amplitude values is calculated. The oscillatory frequency is calculated by the Fast Fourier Transform over the recoded period.

7.1.3 Oscillators and reference Pitot tube

A simple schematic of the new single-cylinder VIVACE Converter and details of two oscillators are shown in Figure 7.1. In the new devices, a rigid circular cylinder is

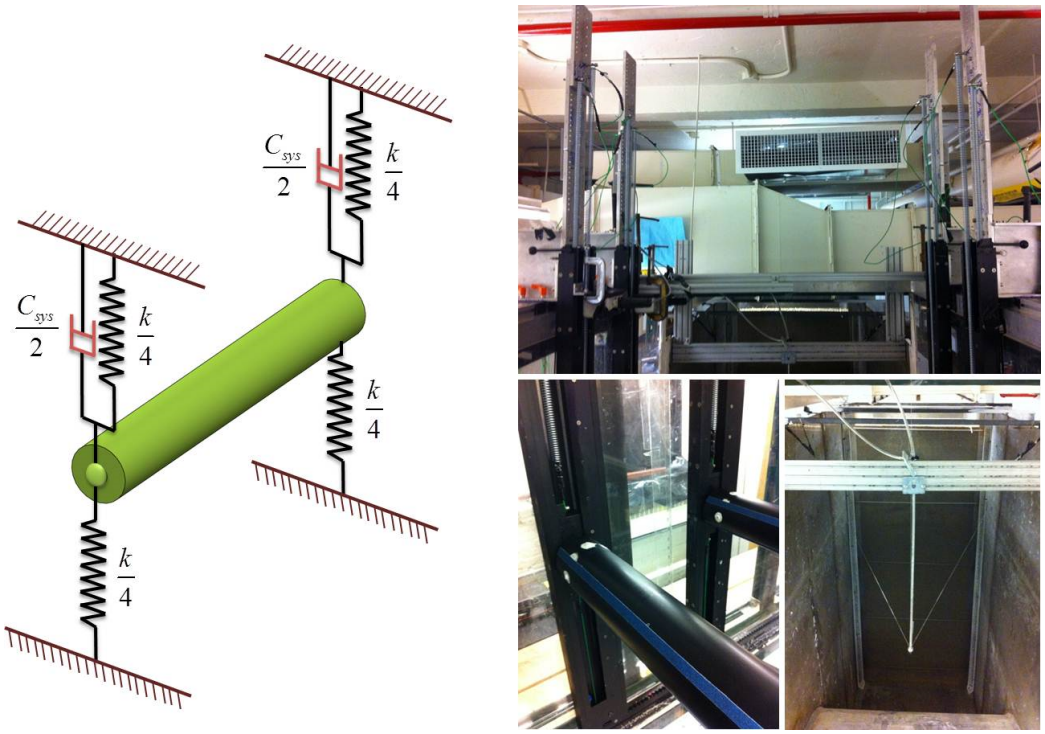

Figure 7.1: Simple schematic of the new VIVACE Converter (left) and details of two-cylinders VIVACE Converter and reference Pitot tube in the new LTFSW Channel (right)

attached to the sliding blocks which are constrained to move transversely to the flow. A linear extension spring is connected at each side of the sliding block and thereby the cylinder-sliding block system is suspended by four linear extension springs while the old device used two linear extension/compression springs. The vertical distance between the cylinders can be set by spring mount systems, which are adjustable by 25.4mm (1") increment. The longitudinal center-to-center distance between the cylinders is adjustable in increments of 12.7mm (0.5") starting at $1.43D$ (D=3.5") using the notches of the new rail system. The details of the new device were presented in Chapter 5. The reference Pitot tube is placed at the entrance of the test section permanently to measure the free stream velocity and at the same time to monitor the reliability of the V_{mean} - f_{motor} relationship which was proposed in Chapter 6. Stiffness of springs and system damping are measured by a series of free decay tests in air. In this chapter, all tests have been done with real extension springs and two

identical circular cylinders made by 6061 aluminum alloy. The diameter and length of the cylinder is 0.089m (3.5") and 0.889m (35"), respectively. The added mass coefficient is assumed to be the ideal flow added mass coefficient which is equal to 1.0.

7.1.4 Passive turbulence control

The effect of the Passive Turbulence Control (PTC) on FIMs of multiple-cylinders was investigated in Part A. In this chapter, for all tests with PTC, the 0.5" wide roughness strip P60 is attached starting at 30° from upstream stagnation point symmetrically on both sides of the cylinder. The details of the P60 PTC are shown in Table 3.2.

7.2 Effect of Spacing of Two Smooth Cylinders in Tandem on FIM

FIM of two smooth cylinders in tandem has been studied experimentally in Chapter 4 and was discussed further with observations by other researchers in Section 5.1.6. In this chapter, the effect of spacing on two smooth cylinder in tandem is investigated further experimentally with the lower mass ratio and a closer longitudinal distance compared to the experimental conditions in Chapter 4. Tests are conducted with two different spring stiffness values and the results are compared with the previous observations.

7.2.1 Experimental setup

Two identical rigid cylinders arranged in tandem are free to oscillate transversely to the flow. The longitudinal center-to-center spacing between the two PTC-cylinders, d/D, is changed from $1.43D$ to $4.0D$. Details of experimental setups are described in

in Table 7.1.

Table 7.1: Details of experimental conditions

SETUP 1	m (kg)	k (N/m)	C (Ns/m)	m^*	ζ	fn,w
1st Device	3.400	290.30	2.870	0.634	0.0456	0.917
2nd Device	3.420	287.52	2.737	0.640	0.0436	0.911
			Parameter			
d/D	1.43	2.00	2.57	3.00	3.57	4.00
SETUP 2	m (kg)	k (N/m)	C (Ns/m)	m^*	ζ	fn,w
1st Device	3.425	524.21	2.276	0.641	0.0267	1.230
2nd Device	3.445	528.86	2.289	0.645	0.0268	1.235
			Parameter			
d/D	1.43	2.00	2.57	3.00		

7.2.2 Results and discussion

Figures 7.2and 7.3 show the amplitude ratio, A/D, and frequency ratio, $f_{osc}/f_{n,w}$, of both cylinders in two different setups of tests at various U^*. For comparison, responses of the smooth single cylinder are plotted in the figures.

1st Cylinder

The designation 1^{st} and 2^{nd} cylinder indicates the upstream and downstream cylinder, respectively. The A/D results are in good agreement with the measurements in Chapter 4. For $d/D \geq 2.57$, The 1^{st} cylinder is not affected by the presence of the 2^{nd} cylinder and the A/D response of the 1^{st} cylinder in for $d/D \geq 2.57$ follows the single cylinder response. The maximum A/D slightly increases and the upper branch becomes wider with decrease in the spacing. The frequency ratio for $d/D \geq 2.57$ is a little higher than that of the single cylinder. For d/D=2.0, however, the trend deviates compared to the previous results due to the effect of the spring stiffness. For K=290.3N/m, the maximum A/D for d/D=2.0 is 17% higher than that of other

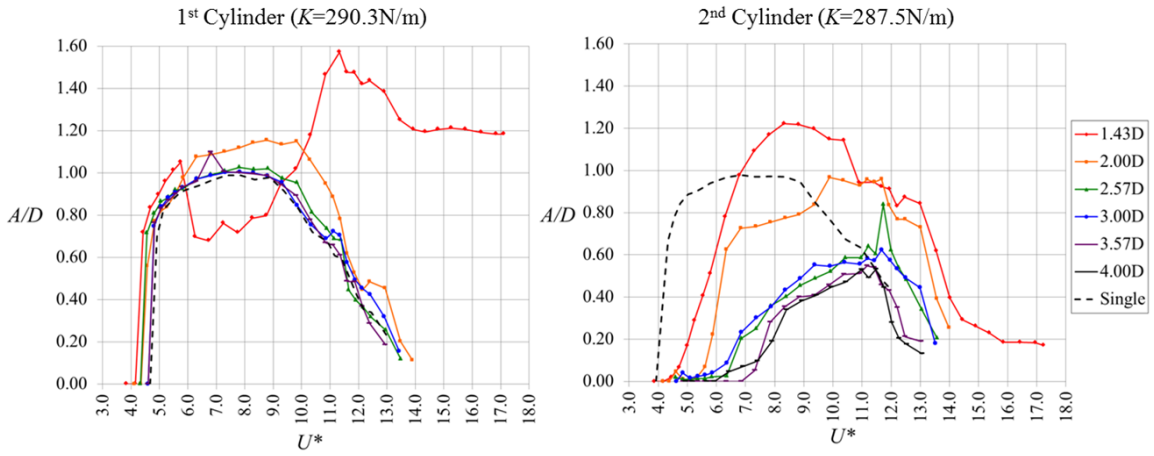

Figure 7.2: Effect of center-to-center spacing of two smooth cylinders in tandem on A/D - Setup 1

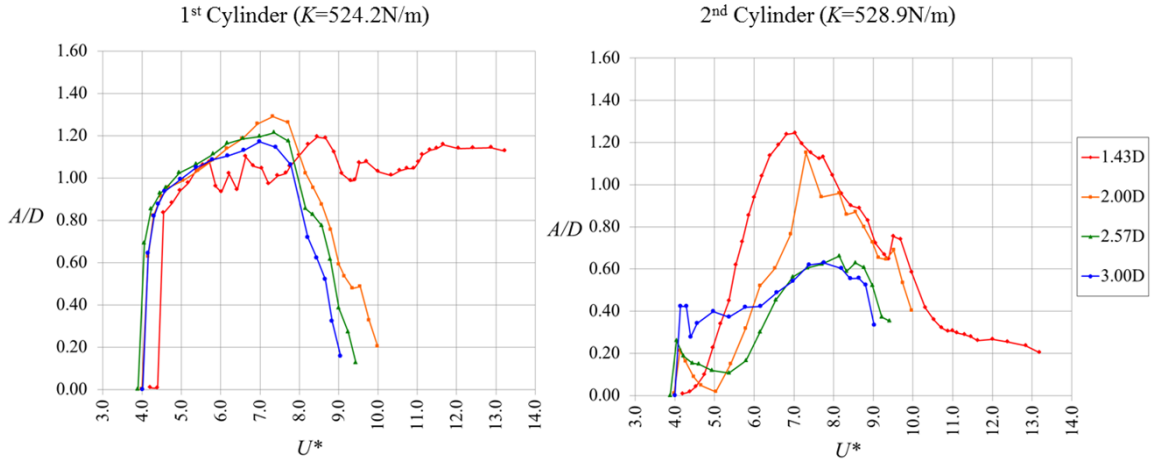

Figure 7.3: Effect of center-to-center spacing of two smooth cylinders in tandem on A/D - Setup 2

spacings as shown in Figures 7.2 and 7.3, while in the previous tests it was smaller compared to other spacings as shown in Figure 4.1. This discrepancy becomes smaller with increase in the spring stiffness as shown in Figures 4.1, 7.2 and Figures 7.3. The maximum A/D increases and the upper branch becomes narrower with increase in the spring stiffness. For K=744.3N/m, 524.2N/m and 290.3N/m, the maximum A/D is 1.69, 1.17, 1.00, respectively. This trend was also observed in experiments of a single

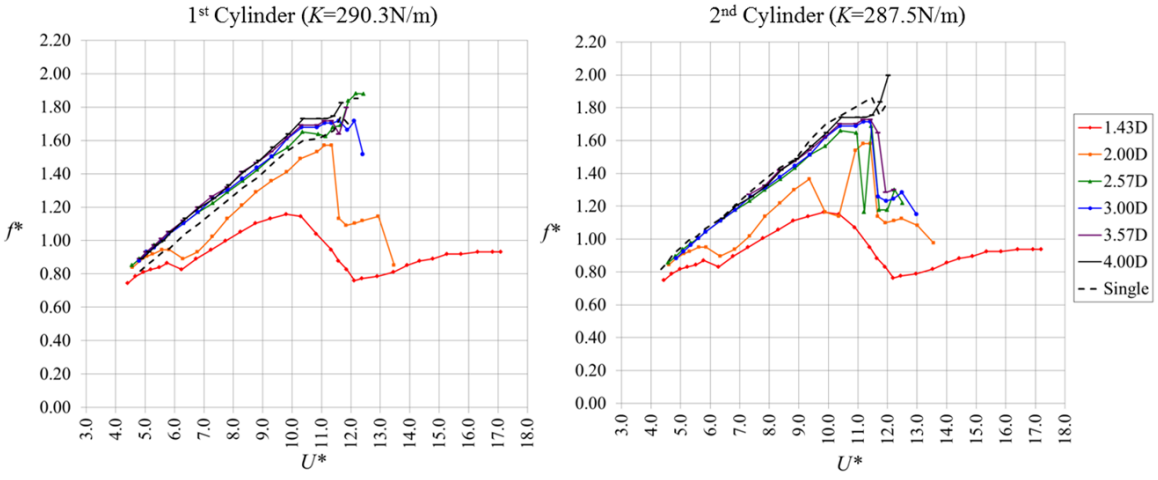

Figure 7.4: Effect of center-to-center spacing of two smooth cylinders in tandem on f^* - Setup 1

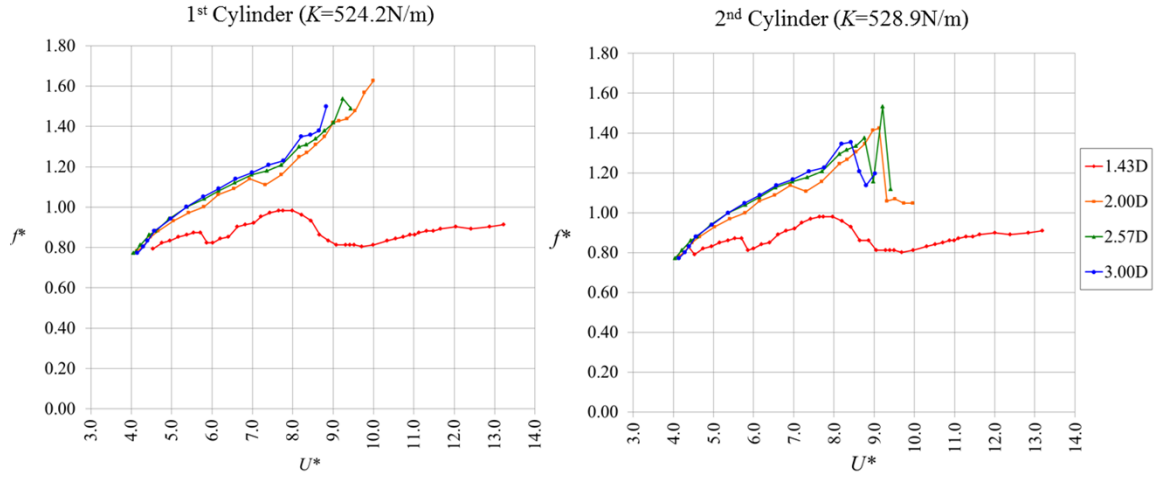

Figure 7.5: Effect of center-to-center spacing of two smooth cylinders in tandem on f^* - Setup 2

smooth cylinder by Lee (2010[19]). The frequency ratio at this spacing is lower than that of other spacings and the discrepancy increases as the spring stiffness decreases as shown Figures 7.4 and 7.5. The response for d/D=1.43 will be discussed separately later in this section. An interesting point is that the oscillation of the 1^{st} cylinder starts around U^*=4.0 regardless of the spacing and spring stiffness. It means that initiation of VIV only depends on the U^*.

2nd Cylinder

The trend of response of the 2^{nd} cylinder is very different from the results of the 1^{st} cylinder. For $d/D \geq 2.57$, the oscillatory amplitude in the upper branch was suppressed and the maximum A/D and synchronization region decrease with increasing in the spacing as shown Figures 4.1, 7.2, and 7.3. The maximum A/D occurs at higher U^* as the spring stiffness decreases. For two high spring stiffness, the first A/D bump appears in the region of $4.5 < U^* < 7$. This is due to the change of vortex shedding mode in the upstream cylinder from 2S to 2P. This phenomenon was investigated by some researchers (Zdravkovich and Pridden, 1977; Brika and Laneville, 1999; Laneville and Brika, 1999; Kim et al. (2009)). Laneville and Brika conducted experiments with two flexible cylinders in tandem arrangement and both free to vibrate with various longitudinal spacing values in a wind tunnel. They measured the amplitude response of both cylinders and the phase angle between vortex shedding from the upstream cylinder and the displacement of the downstream cylinder. They observed three discontinuities in the amplitude response of the downstream cylinder as shown in Figure 7.6. The first discontinuity concurs with that of the upstream cylinder where the vortex shedding mode of upstream cylinder changes from 2S to 2P. At this point the phase jumps from -135° to 0°. The second discontinuity happens at the end of the upper branch of the upstream cylinder and it is only clearly observed in the previous tests shown in Figure 4.1. The third one occurs at the end of the lower branch and it is not observed in the author's tests because the lower branch is not

clearly shown in the results. It is observed that the amplitude bump decreases as the longitudinal spacing increases both in Laneville and Brike, and the author's tests. For K=287.5N/m, the first discontinuity is still observed in the amplitude response of the 2^{nd} cylinder but the A/D around U^*=5 is very small compared to that of other spring stiffness. The oscillatory frequency of the 2^{nd} cylinder is almost synchronized with that of the 1^{st} cylinder and shows fluctuation only near the end of the lower branch. The amplitude of the 2^{nd} cylinder is lower compared with the results shown in Chapter 4. This could be due to the effect of the under water structures. The under water structures disturb the flow and the flow becomes highly 3-dimensional and the separation of the boundary layers on the 2^{nd} cylinder is not parallel to the cylinder axis. This oblique separation can decrease the lift force on the cylinder.

Response of two cylinders in tandem for spacing of d/D = 1.43

For d/D=1.43, the amplitude and frequency response of both the 1st and 2nd cylinder are very different from those of other spacings. This is because of the effect of the strong wake interference between the two cylinders. Zdravkovich (1987) classified five different regimes of the wake interference for two cylinders in tandem arrangement based on behavior of the free shear layer and vortex shedding; (a) Single slender body, (b) Alternate reattachment, (c) Quasi-steady reattachment, (d) Intermittent shedding, and (e) Two vortex street regimes. Kim et al. (2009) identified their own five regimes which depend on the L/D, fluctuating lift force and vibration characteristics. Here L indicates the gap between cylinders rather than the distance between centers of cylinders, d/D, used in this dissertation (d/D=1+L/D). They visualized the flow structures of two oscillatory cylinders in different regimes as shown in Figure 7.7. The spacing of d/D=1.43 is in Regime II based on Kim et al.'s classification. In this regime, two shear layers separate from the upstream cylinder, reattach to the surface of the downstream cylinder and finally, a Karman vortex street is formed behind the downstream cylinder. One of the free shear layers separates from

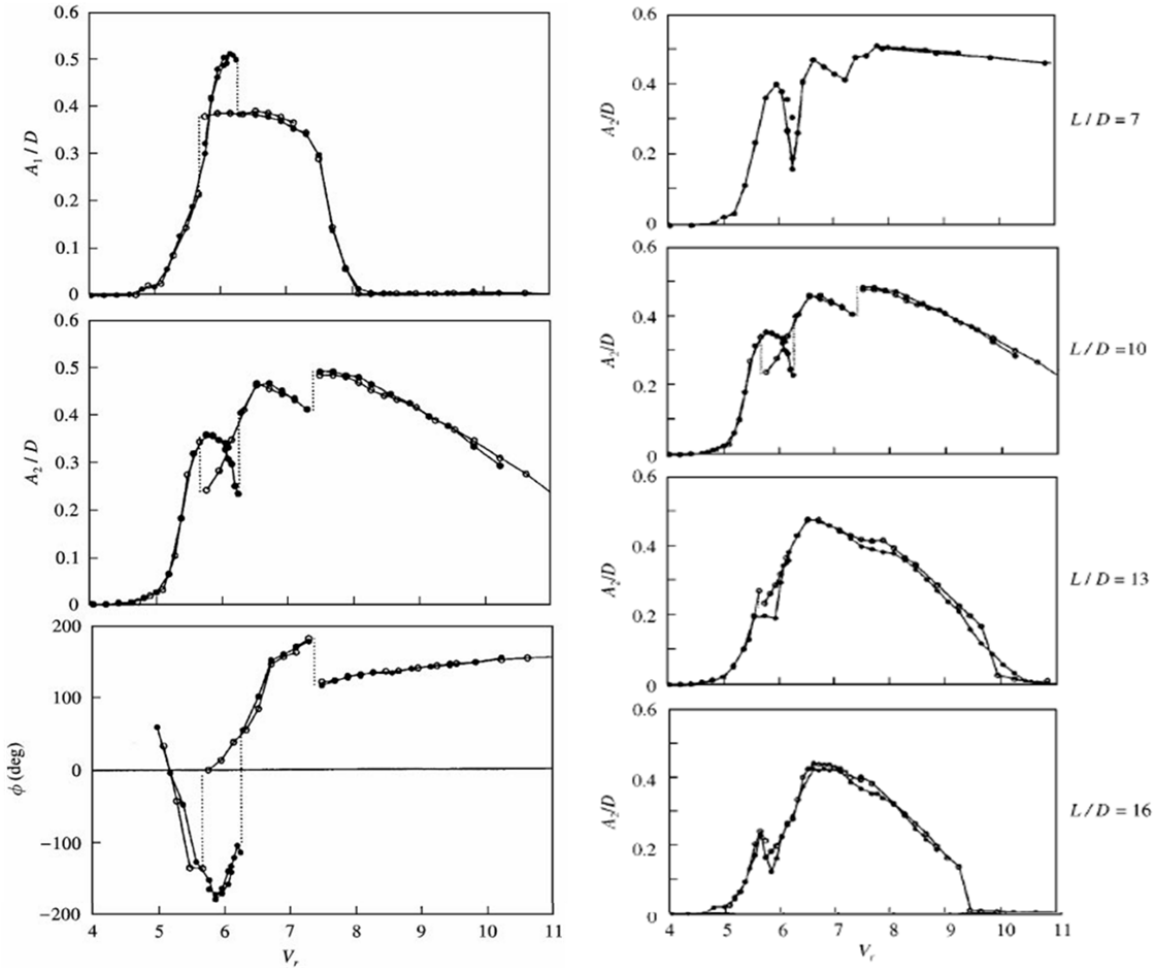

Figure 7.6: Response of upstream (A_1/D) and downstream (A_2/D) cylinders and phase difference between vortex shedding from upstream cylinderand the response of the downstream cylinder; d/D=10 (left) and response of downstream cylinder at different tandem spacings (right) [Reproduced from Laneville and Brike, 1999]

the upstream cylinder bifurcates in to two and rolls in the gap between cylinders. This bifurcation causes an unsteady lift on the upstream cylinder.

Alam et al. (2003a) further investigated experimentally the alternate reattachment and quasi-steady reattachment regimes by measuring fluctuating lift and drag forces of two stationary cylinders and vortex shedding patterns at Re=6.5×10^4. As shown in Figures 7.8, they measured the fluctuating lift and drag coefficient of two cylinders in tandem arrangement and a single cylinder at various tandem spacings. Before discussing the results it is important to be noted that the characteristics of the flow regimes depend on Reynolds number (Gartshore, 1984; Xu and Zhou, 2004). These results show that the fluctuating lift force of both cylinders depend on the tandem spacing and it changes dramatically in the region of $0<L/D<$ 2.0. Their testing Reynolds number corresponds to U^*=10.9 and 8.5 for the experimental Setup 1 and 2, respectively. The trend in the fluctuating lift and drag coefficient plots of two stationary cylinders corresponds well with author's A/D plots. In the plot of the fluctuating lift coefficient the first peak appears at L/D=0.4 where the fluctuating drag coefficient of the upstream cylinder is relatively low. At this spacing, the A/D of the 1^{st} cylinder shows almost its maximum values in the author's tests for both experimental setups 1 and 2 at L/D=0.43 (d/D=1.43). The amplitude response depends on both the fluctuating lift and drag forces so even though the higher fluctuating lift coefficient of the downstream cylinder at this spacing is much higher than that of the upstream cylinder, the A/D of the 2nd cylinder is lower than that of the 1^{st} cylinder due to the relatively high fluctuating drag coefficient. This feature was also observed by Kim et al. (2009).

There are, however, some discrepancies between their results and the author's results. First, the A/D is much lower than that of author's tests as shown in Figure 7.9. Second, the A/D of both the upstream and the downstream cylinders is higher than that of L/D=1.0 in the range of $1.2<L/D<$ 1.8. As shown in Figure 7.2,

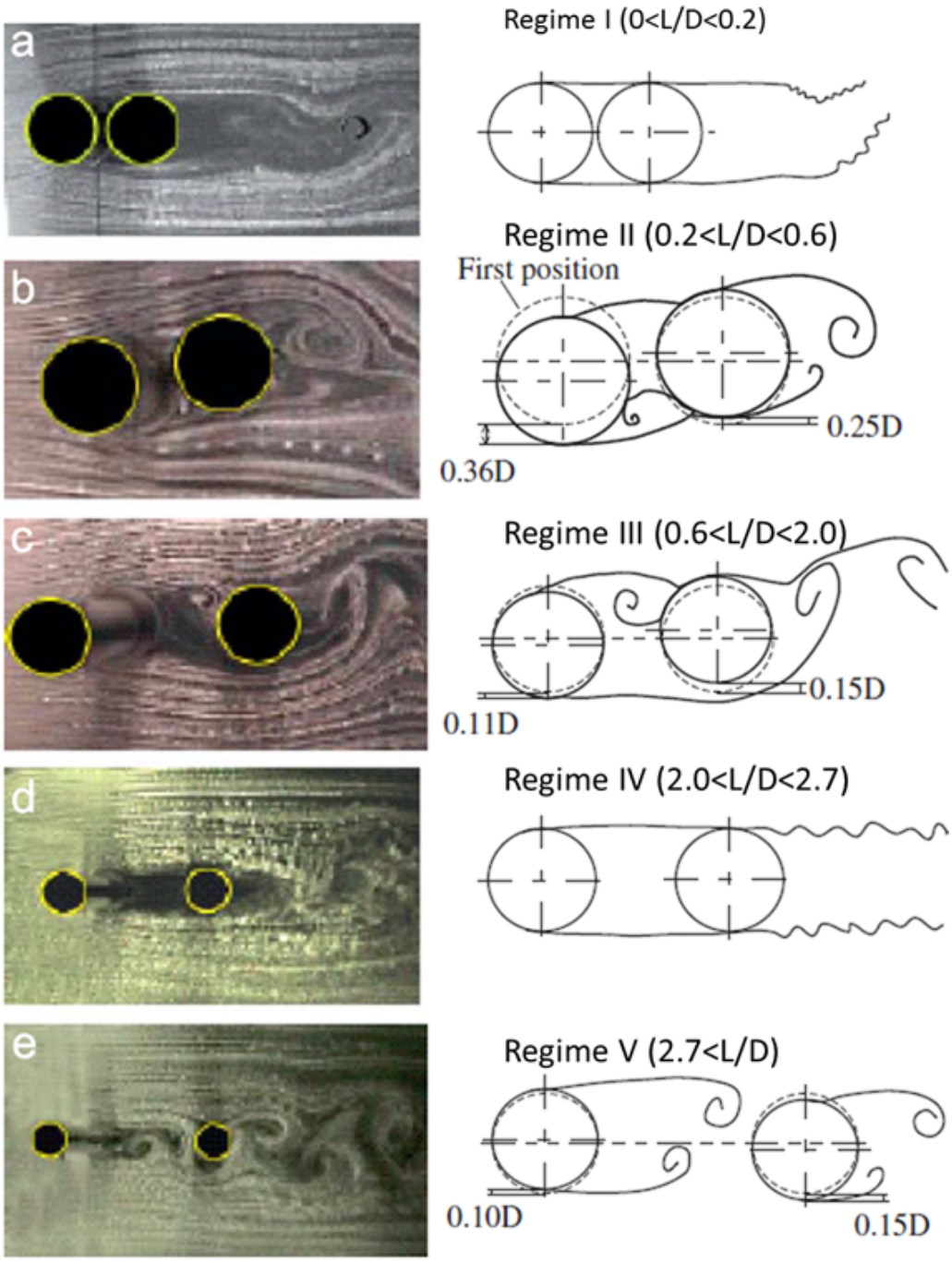

Figure 7.7: Visualized flow structures and corresponding sketches: (a) L/D=0.1, (b) L/D=0.3, (c) L/D=1.5, (d) L/D=2.0, and (e) L/D=3.2 [Reproduced from Kim et al, 2009]

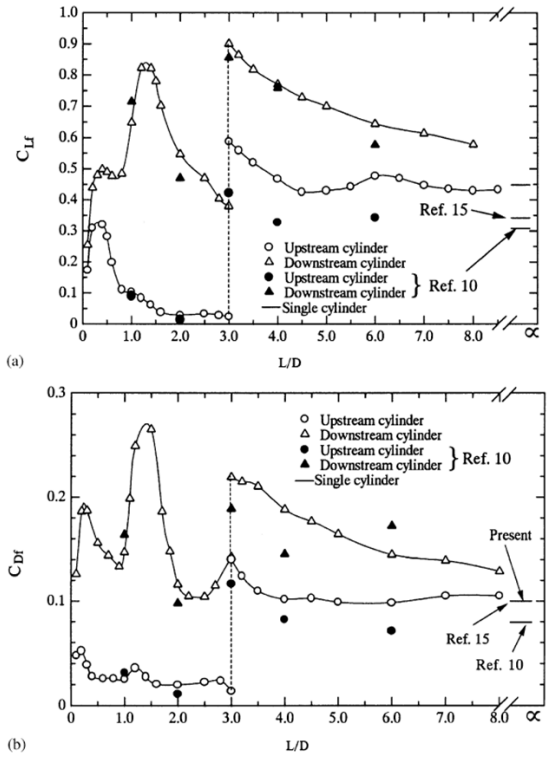

Figure 7.8: Variation in fluctuating fluid forces with increase in tendem spacing (L: gap spacing, D: diameter of cylinder); (a) fluctuating lift coefficient, (b) fluctuating drag coefficient [Reproduced from Alam et al., 2003a]

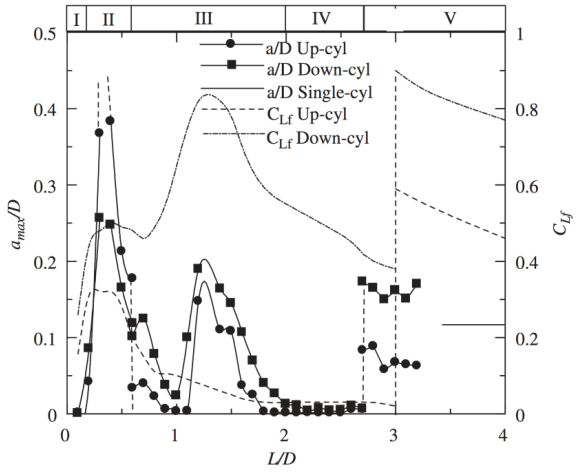

Figure 7.9: Amplitude response of two oscillatory cylinders in various tandem spacing [Reproduced from Kim et al, 2009]

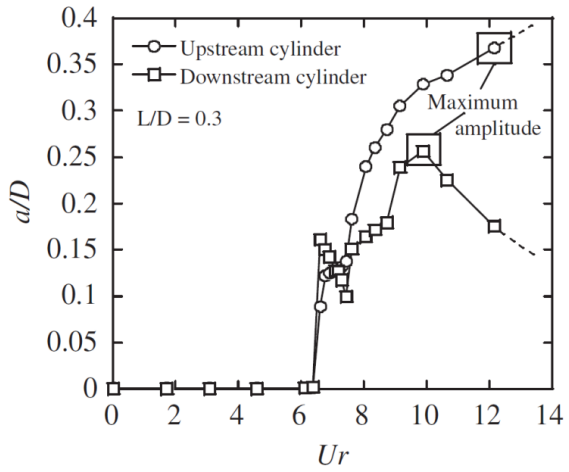

Figure 7.10: Amplitude response of two oscillatory cylinders for various Reduced velocity; L/D=0.3 [Reproduced from Kim et al, 2009]

the A/D of both 1^{st} and 2^{nd} cylinders decreases with increasing L/D in this region. This is because of the difference in the mass-dapping ratio. They used the reduced mass-damping factor, $Cn = 2m\delta/(\rho D^2)$ where m is the cylinder mass per unit length and δ is the logarithmic decrement, rather than the traditional mass-damping ratio. Their reduced mass-damping factor is 6.36 while it is between 0.259 and 0.267 in the author's tests. As the mass-damping ratio decreases, A/D increases and at the same time the upper branch becomes wider (Govardhan and Williamson, 2002).

Kim et al. (2009) also investigated the cylinder response at various reduced velocity values, U^*, as shown in Figure 7.10. Their results show that for L/D=0.3, the A/D of the upstream cylinder gradually increases up to U^*=12 while the A/D of the downstream starts to decrease beyond U^*=10. This tendency is also observed in Figures 7.2 and 7.3. For the experimental setup 1, the A/D of the 1^st cylinder reaches its maximum value of 1.57 at U^*=11.2 and then its value decreases to 1.2 in the range of 11.2$< U^* <$14.0. TheA/D of the 1st cylinder remains unchanged until U^* reaches the allowable limit of the facility. For the Setup 2, the A/D of the 1st cylinder also shows somewhat similar trend and the value of A/D reaches and remains at almost 1.2 for $U^*>$11.5. For both setups 1 and 2, the oscillation of the 2nd cylinder gradually

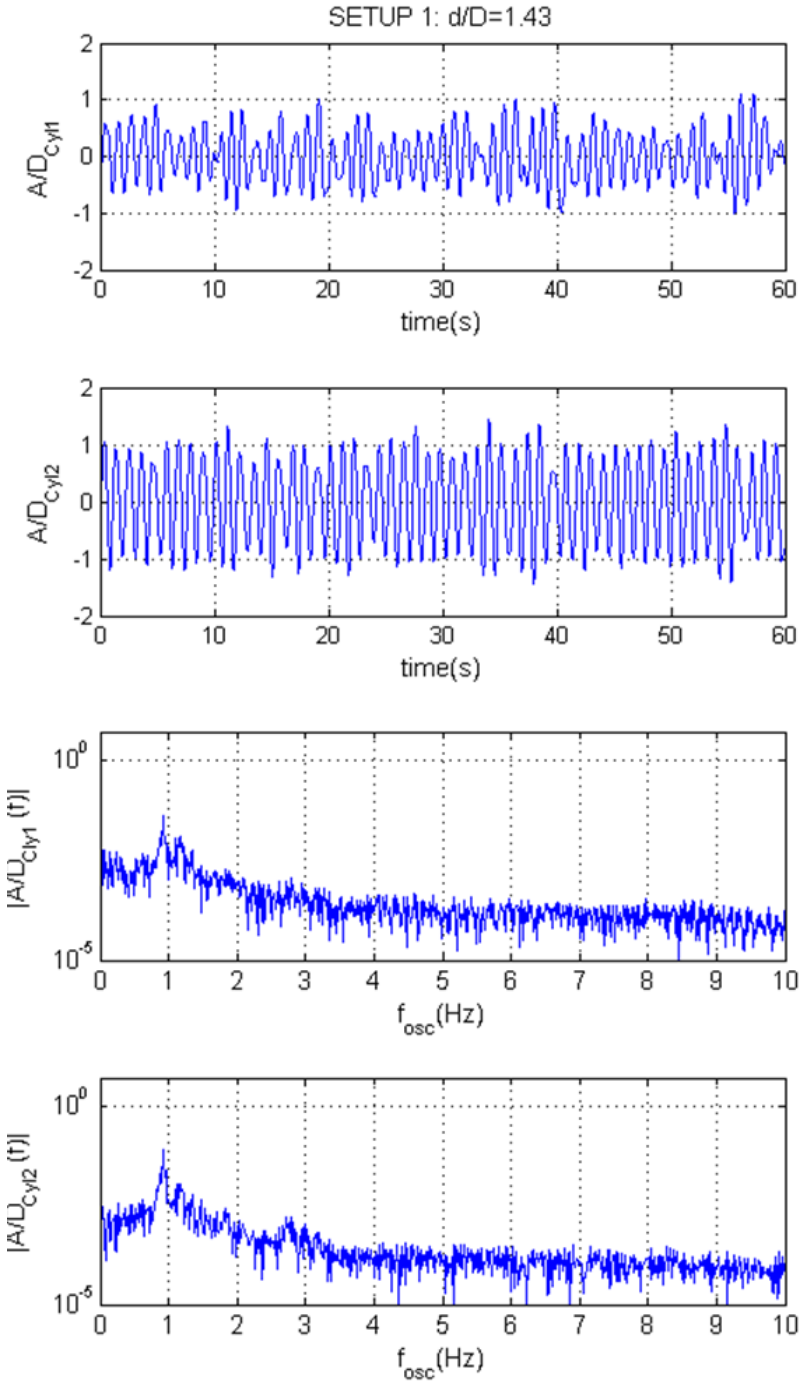

Figure 7.11: Beating FIM phenomenon of two cylinders in tandem; L/D=1.43 and U^*=7.75

increases without any discontinuity until its maximum A/D of 1.24 and then keeps decreasing at the end of desynchronization.

A discontinuity is observed around U^*=5.5 in the A/D plots of the 1st cylinder where the vortex shedding mode changes from 2S to 2P. The phase between the 1st and 2nd cylinder oscillation keeps changing from in phase to out of phase. The beating phenomenon was observed in the amplitude time history plots of both cylinders in the region of $6.0<U^*<9.0$ as shown in Figure 7.11. In this region, the 2nd cylinder has higher oscillatory amplitude compared to the 1st cylinder and forms its own vortex shedding, while the vortex shedding of the 1st cylinder is suppressed by the oscillation of the second cylinder and thereby the oscillatory amplitude of the 1st cylinder also suppressed.

The oscillatory frequency of both 1st and 2nd cylinders is synchronized and much lower compared to that of wider spacings as shown in Figures 7.4 and7.5. The frequency ratio gradually increases with increase in U^* and it slightly drops around U^* =6.0 where the change in the vortex shedding mode occurs. It decreases in the region of $10<U^*<12$ which is the end of the upper branch. The frequency ratio gradually increases again near the natural frequency of the system in water like galloping.

As we discussed in this section, the response of two oscillatory cylinders in tandem arrangement are very interesting and especially, for $d/D<2.0$, the results are distinguishing. In this rang of the spacing, the fluctuating lift and drag forces are dramatically change due to the flow structures sensitively change with the spacing. However, only one spacing of d/D=1.43 was tested in this dissertation and more observation are needed with visualization to understand the flow structures in the region of $d/D<2.0$.

7.3 Effect of Tandem Spacing on FIM of Two Cylinders with PTC

The effects of PTC and tandem spacing on FIM of multi-cylinders have been investigated in Chapter 4. By introducing PTC, all multi-cylinders were able to achieve back-to-back VIV and galloping with high amplitude response no matter how close the cylinders were. Moreover, the upstream cylinder was not significantly affected by the presence of the downstream cylinders. In this section, the effect of tandem spacing is further investigated with a closer spacing and three different spring stiffness values.

7.3.1 Experimental setup

For all tests, the half-inches wide P60 strips were attached starting at 30 degrees from upstream stagnation point symmetrically on both sides of the cylinder. The d/D was changed from 1.43 to 4.0. All tests were conducted in the LTFSW Channel in the range of 0.32m/s$<U<$1.39m/s and 23,000<Re<104,000. Details of the experimental setups are described in Table 7.2.

7.3.2 Results and discussion

***A/D* of the 1^{st} cylinder: Figures 7.12 to 7.14**

- A/D response is distinguished by the spacing of d/D=2.0.
- For $d/D\geq$ 2.0,A/D response in VIV is similar for all spacings and not significantly affected by the presence of the downstream cylinder. VIV initiates at $U^* \approx 4.0$.
- For d/D=1.43, VIV starts at higher U^* and A/D in the initial branch is smaller than that of other d/D values.

- For all spacing and spring stiffness values, A/D in the upper branch gradually increases with increasing U^* and reaches its maximum value of 0.85-0.99.
- Transition from VIV to galloping starts earlier as d/D decreases and for K=286 and 800N/m, separation between the upper branch and galloping was observed as d/D increases and at this point A/D dramatically drops and then shoots up. For d/D=1.43 and 2.00, no separation was observed.
- In the fully galloped region, for K=280N/m, A/D reaches up to 2.89 3.36 and for the two closest d/D values A/D is lower in this region but as K increases the discrepancy decreases.
- For d/D>2.0, the upper branch is clearly separated from galloping in the Setup

Table 7.2: Details of experimental conditions

SETUP 3	m (kg)	k (N/m)	C (Ns/m)	m^*	ζ	fn,w
1st Device	3.400	285.95	2.398	0.634	0.0384	0.910
2nd Device	3.420	284.99	2.307	0.640	0.0370	0.908
			Parameter			
d/D	1.43	2.00	2.57	3.00	3.57	4.00
SETUP 4	m (kg)	k (N/m)	C (Ns/m)	m^*	ζ	fn,w
1st Device	3.425	522.66	2.293	0.641	0.0267	1.228
2nd Device	3.445	528.88	2.715	0.645	0.0318	1.236
			Parameter			
d/D	1.43	2.00	2.57	3.00	3.57	4.00
SETUP 5	m (kg)	k (N/m)	C (Ns/m)	m^*	ζ	fn,w
1st Device	10.203	800.18	5.274	1.663	0.0292	1.145
2nd Device	10.198	794.04	6.123	1.662	0.0340	1.141
			Parameter			
d/D	1.43		2.00	3.00		4.00

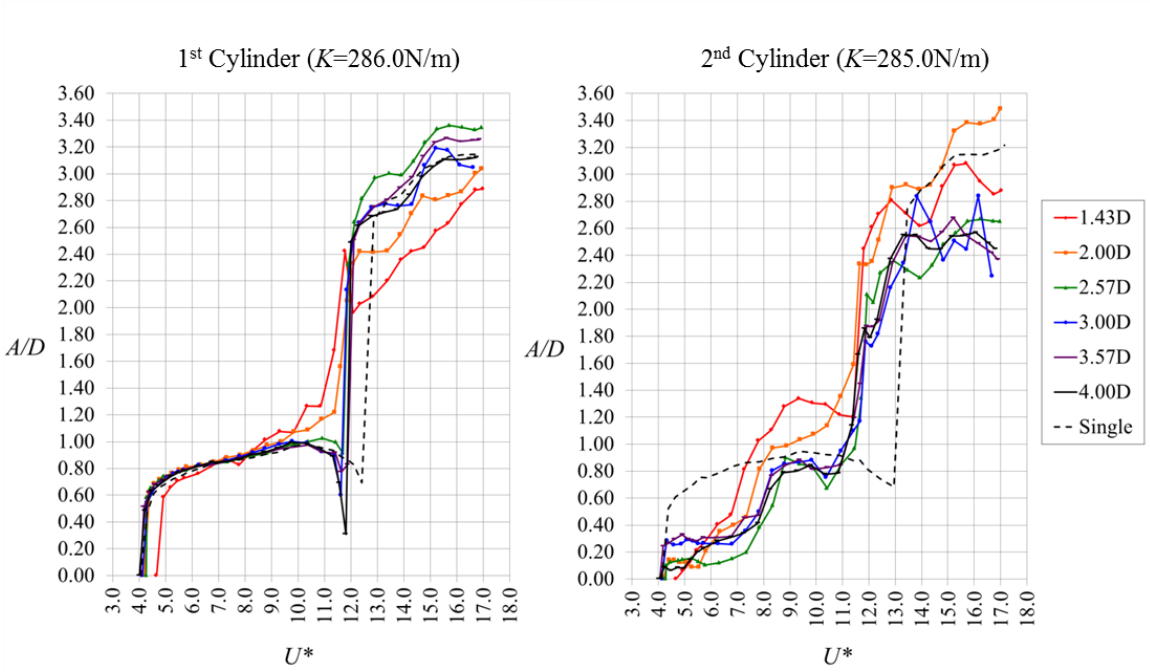

Figure 7.12: Effect of center-to-center spacing of two PTC-cylinders in tandem on A/D - Setup 3

3. At U^*=12 there is a big drop just before initiation of galloping, whereas A/D of the Setup 4 doesn't show any drop between the upper branch and the initiation of galloping.

- For d/D=1.43 and 2.00, A/D of the first cylinder is lower than those of the 2^{nd} cylinder in galloping.

A/D of the 2^{nd} cylinder: Figures 7.12 to 7.14

- The 2^{nd} cylinder is in the wake of the 1^{st} cylinder and its A/D is much lower.
- A/D starts to increase from U^*=7 where the A/D of the 1^{st} cylinder is greater than 0.8. As shown in the frequency plot, the oscillatory frequency of the 2^{nd} cylinder follows the frequency of the 1^{st} cylinder and is separated from it at U^*=7 or 8 where the A/D of the 1^{st} cylinder passes 0.8. The 2^{nd} cylinder experiences its own VIV until U^*=10.

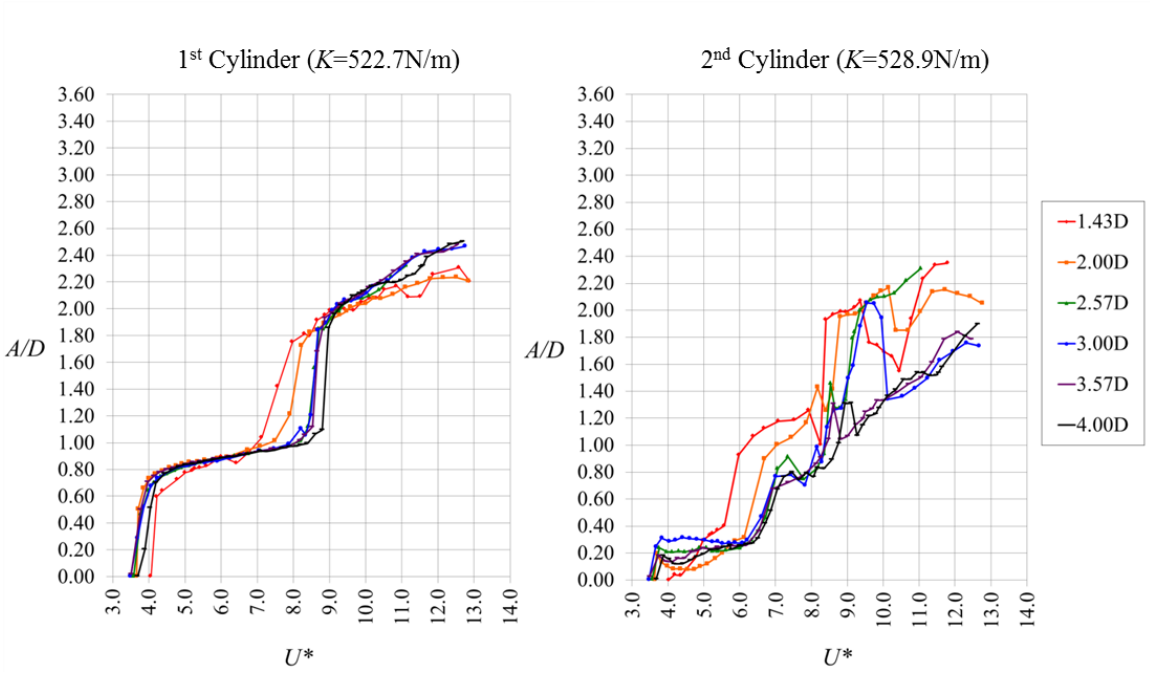

Figure 7.13: Effect of center-to-center spacing of two PTC-cylinders in tandem on A/D - Setup 4

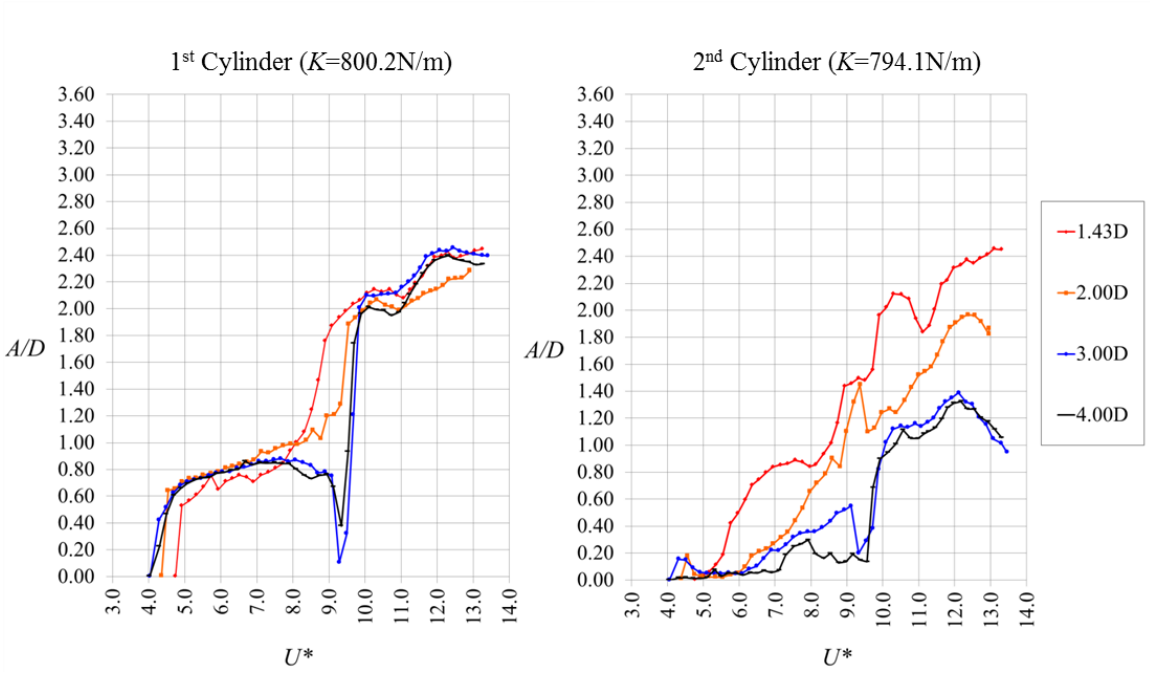

Figure 7.14: Effect of center-to-center spacing of two PTC-cylinders in tandem on A/D - Setup 5

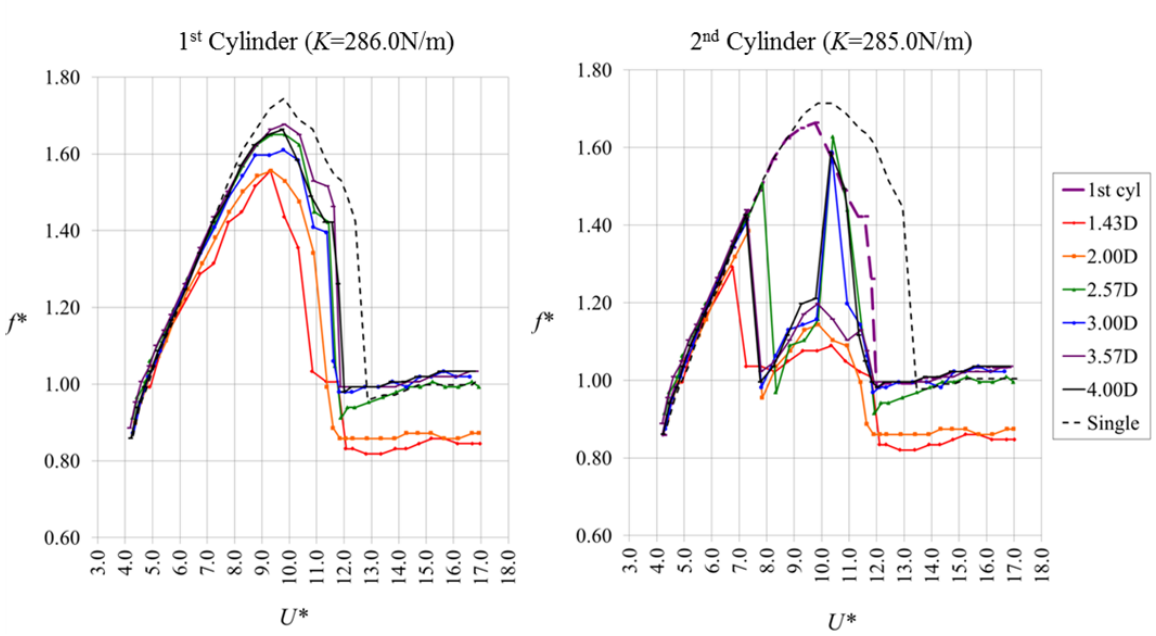

Figure 7.15: Effect of center-to-center spacing of two PTC-cylinders in tandem on f^* - Setup 3

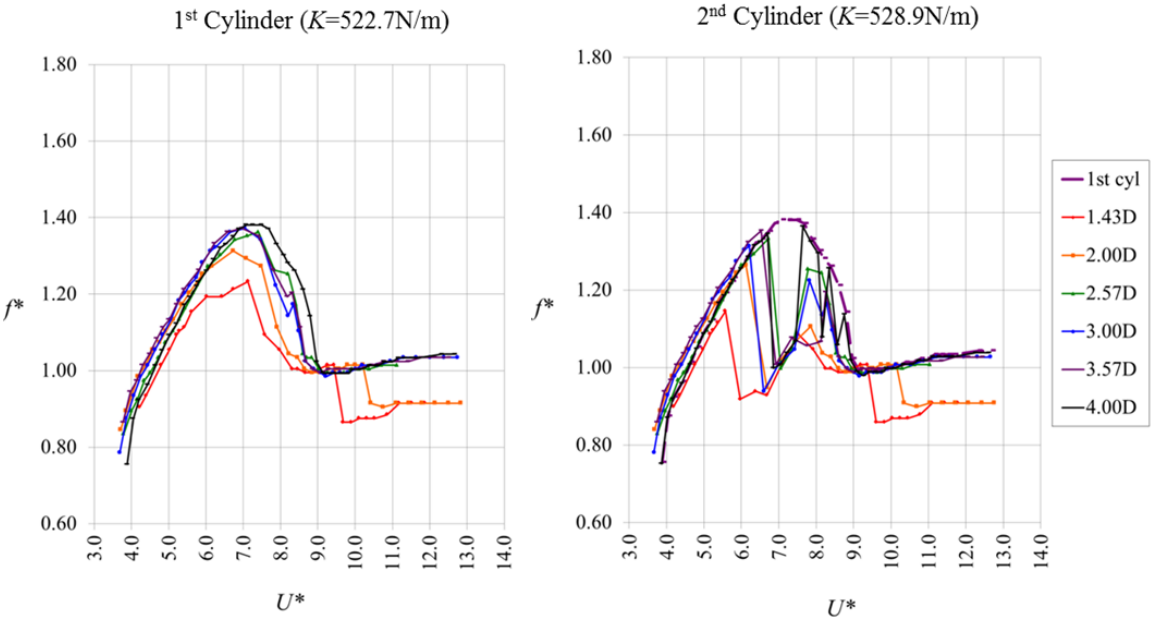

Figure 7.16: Effect of center-to-center spacing of two PTC-cylinders in tandem on f^* - Setup 4

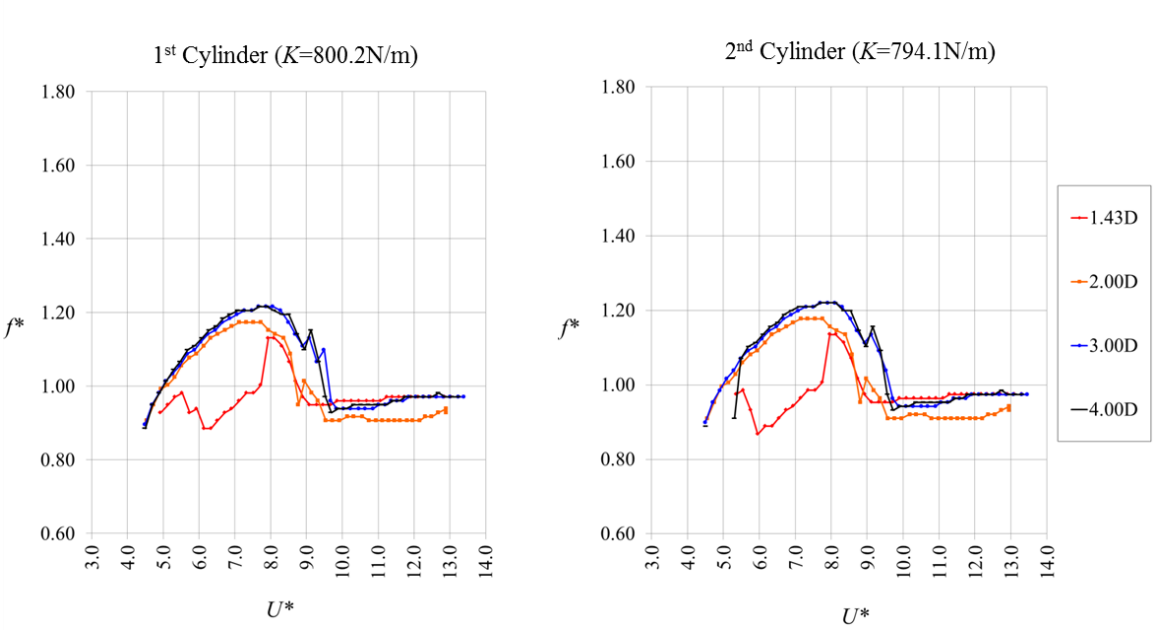

Figure 7.17: Effect of center-to-center spacing of two PTC-cylinders in tandem on f^* - Setup 5

- For d/D=1.43, A/D is higher than those in the other cases from U^*=6 and reach its maximum value 1.27 and 1.38 at U^*=8 and 9.3 for K=528.99N/m and 284.99N/m, respectively. For K=284.99N/m, the amplitude gradually decreases and reaches 1.20 at U^*=11.5 before galloping is initiated.

- Galloping of the 2^{nd} cylinder starts at U^*=10.5 11, while it starts at U^*=12 for the 1^{st} cylinder.

- Fluctuation of A/D of the 2^{nd} cylinder in galloping is bigger than that of the 1^{st} cylinder.

- Maximum A/D of the 2^{nd} cylinder in galloping is lower than that of the 1^{st} cylinder except for d/D=1.43 and 2.00.

- For d/D=1.43 and 2.00, the amplitude responses are very different from those of the wider spacings. The A/D of the two closest cases are much higher from

U^*=6.0 than those of other cases and max A/D of d/D=2.0 reaches 3.5 which is even bigger than any max A/D of the 1^{st} cylinder in galloping.

- Amplitude response of the 2^{nd} cylinder decreases as the tandem spacing increase in galloping. This is different from the results in Chapter 4. In Chapter 4, the oscillatory amplitude of the 2^{nd} cylinder didn't vary much with the tandem spacing for $d/D \geq 3.0$ and the maximum A/D was almost same with that of the 1^{st} cylinder. This may be the effect of air bubbles in the water. As shown in Figure 7.18, the air bubbles start to appear in the flow and their fraction increases with increasing velocity and the flow becomes two phase of water and air bubbles. Hara and Iijima (1988) studied experimentally the effect of air bubbles in cross flow on the vibrational response of two cylinders in tandem, having the tandem spacing of d/D=3.0. They conducted experiments by changing the air bubble fraction in water flow from 0% to 20% for various U^* and two cylinder were allowed to oscillate in both lift and drag directions. They concluded that (i) the air bubbles increase the vibrations of both cylinders for $U^* < 3$, (ii) the air bubbles enhance the oscillation of the upstream cylinder for $3 < U^* < 4$, and (iii) for $U^* > 4$, a small amount of the air bubbles suppressed the large lift direction of oscillation especially of the downstream cylinder as shown in Figure 7.19. They presumed that the large amount entrainment of the air bubbles within the region between the two cylinders suppress the large lift direction of oscillation of downstream. This can be the reason why the A/D of the 2^{nd} cylinder is suppressed for $d/D \geq 3.0$ in galloping compared to the results in Chapter 4.

f^* of the 1^{st} cylinder: Figures 7.15to 7.17

- Three frequency plots show very similar trend each other.

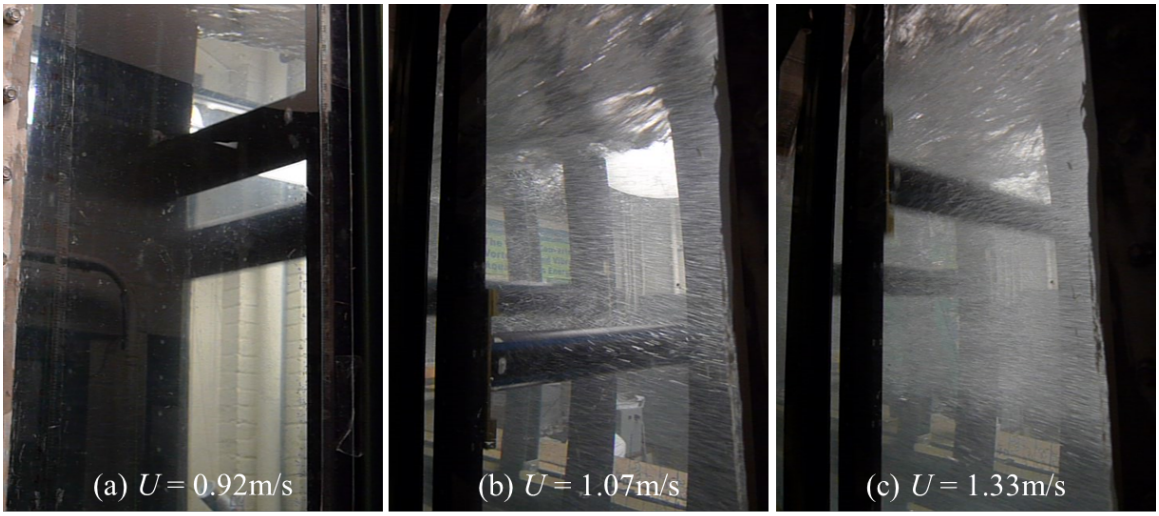

Figure 7.18: Fraction of air bubbles in new LTFSW Channel at various flow speeds; (a) U=0.92m/s, (b) U=1.07m/s, and (c) U=1.33m/s

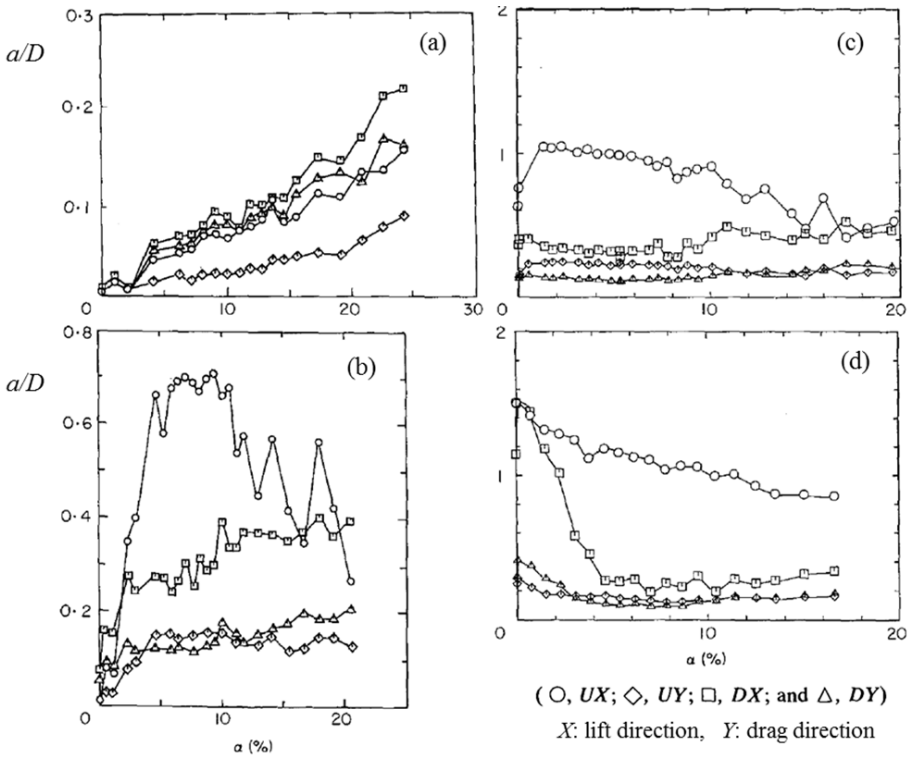

Figure 7.19: Amplitude response of two circular cylinder in tandem arrangement as a function of air bubble fraction; (a) U^*=2.0, (b) U^*=3.48, (c) U^*=4.04, and (d) U^*=7.05

- The frequency ratio increases gradually in VIV and decreases in the transition region from VIV to galloping.

- The 1^{st} cylinder in the fully galloped region oscillates very close to the natural frequency of the system in the water.

- As the tandem spacing decreases, the oscillatory frequency decreases and especially for $d/D \leq$ 2.0, the frequency ratio in the fully galloped region is almost 10 12% lower than that of other spacings. This is because the vortex shedding from the upstream cylinder is suppressed by the 2^{nd} cylinder (Wu et al. 1999; Alam et al. 2003a).

- For the experimental Setup 5, the frequency ratio of d/D=1.43 shows a different trend in the VIV upper branch. For this spacing, the oscillation of the 1^{st} cylinder is significantly affected by the 2^{nd} cylinder and both cylinders show the beating phenomenon. For most of the cases, the vortex shedding frequency of the 1^{st} cylinder is dominant in the beat of the 1^{st} cylinder, but for this case, the oscillatory frequency of the 2^{nd} cylinder is more dominant.

f^* of the 2^{nd} cylinder: Figures 7.15to 7.17

- The oscillation of the 2^{nd} cylinder is significantly influenced by the 1^{st} cylinder regardless of the tandem spacing.

- Due to the effect of the 1^{st} cylinder in the oscillation of the 2^{nd} cylinder, two major frequencies appear in its frequency plot before the fully developed galloping region.

- The oscillatory frequency of the 1^{st} cylinder is dominant in the frequency plots of the 2^{nd} cylinder until the A/D of the 1^{st} cylinder reaches 0.8.

- Once the A/D of the 1^{st} cylinder is larger than 0.8, the oscillation frequency of the 2^{nd} cylinder becomes more dominant than that of the 1^{st} cylinder.
- The frequency fluctuates in the transition region from VIV to galloping.
- In the fully developed galloping region, the trend of the oscillatory frequency is almost same as that of the 1^{st} frequency.

Time history of A/D and frequency plot: Figures 7.20 to 7.26

Time history of the A/D and frequency for d/D=1.43 and 4.0 were plotted at various U^*'s in order to investigate the beating phenomenon.

Figure 7.20: U^*=5.03 (Re=31,000)

- This is in the transition region from TrSL2 to TrSL3 and the initial branch to upper branch of VIV.
- For d/D=1.43 and 4.0, the A/D of the 1^{st} cylinder is 0.691 and 0.742, respectively. For the 2^{nd} cylinders, the A/D is nearly equal to zero.
- Frequency plots of the 2^{nd} cylinders for both spacings shows a peak at the same major frequency of the 1^{st} cylinder due to the wake of the upstream cylinder.
- For d/D=1.43, a super harmonic frequency which is twice of the major frequency is clearly shown in both frequency plots of up and downstream cylinders whereas it is not shown in the plots of d/D=4.0. This super harmonic frequency indicates the alternating free shear attachment effect as discussed in Section 7.3.2 and this feature was also observed by Alam et al. (2003a) as shown in Figure 7.25.

Figure 7.21: U^*=6.83 (Re=42,000)

- This is in TrSL3 region and the upper branch of VIV.

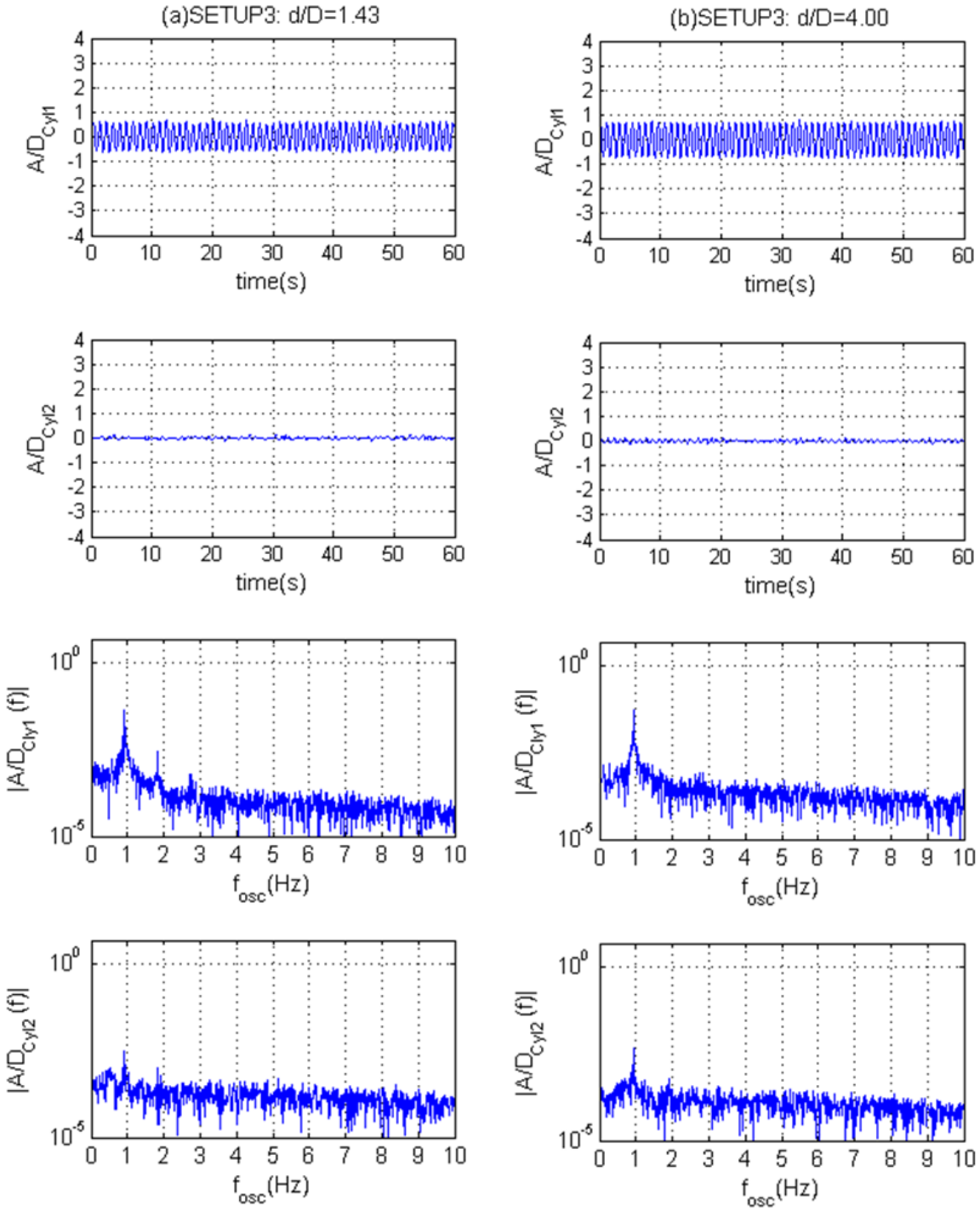

Figure 7.20: U^*=5.03 (Re=31,000); A/D and f_{osc} for d/D=1.43 (a-column) and d/D=4.00 (b-column)

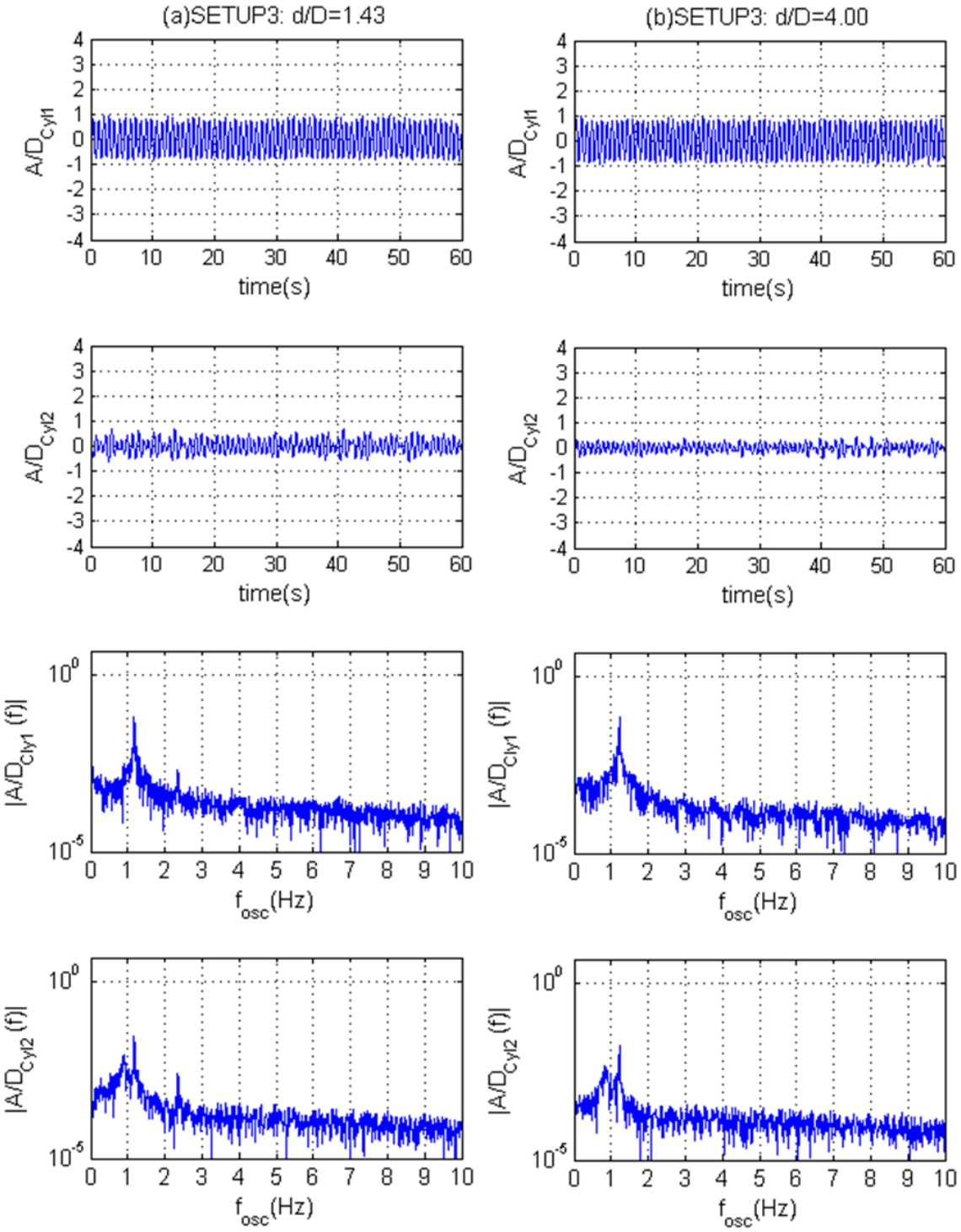

Figure 7.21: U^*=6.83 (Re=42,000); A/D and f_{osc} for d/D=1.43 (a-column) and d/D=4.00 (b-column)

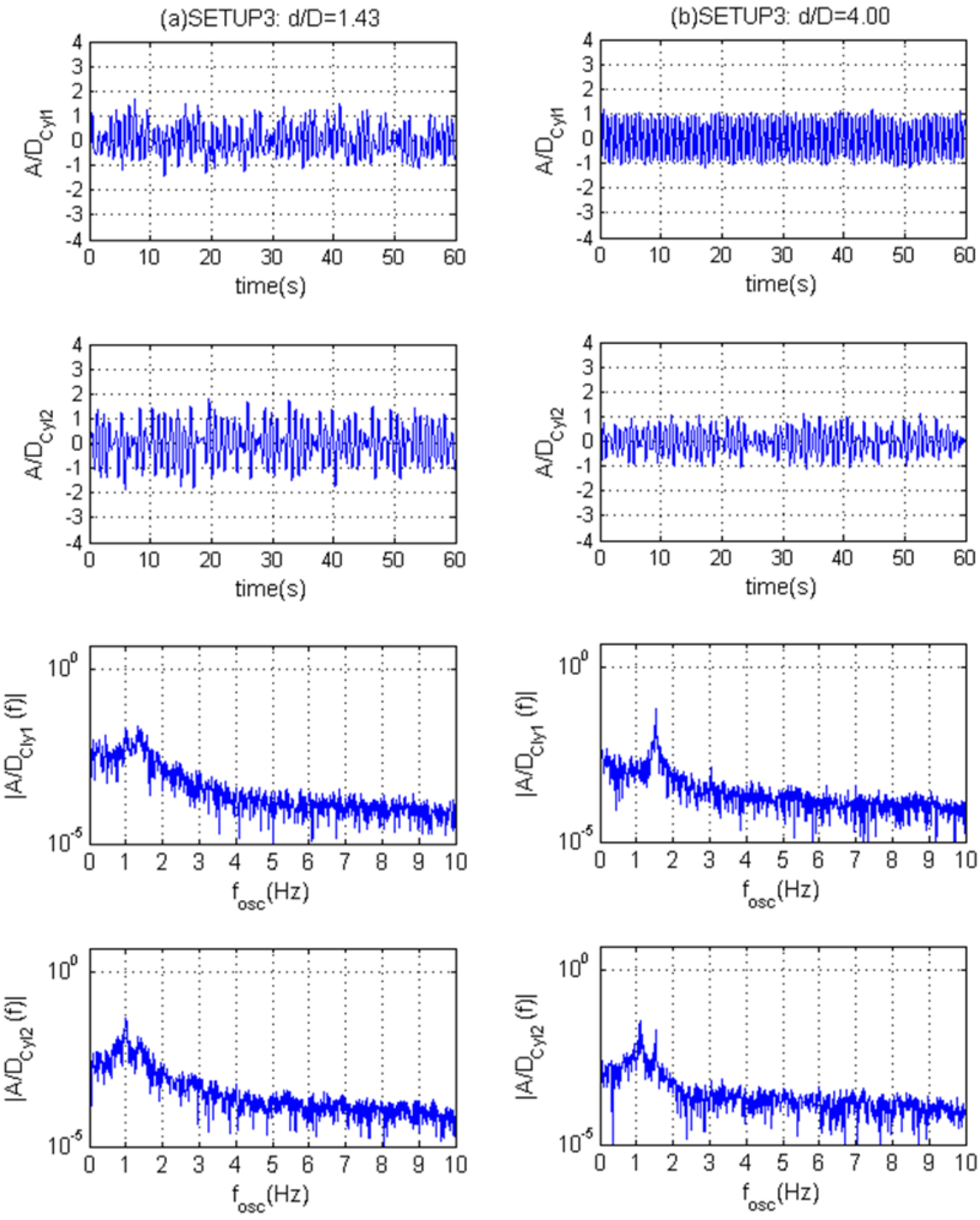

Figure 7.22: U^*=9.89 (Re=60,800); A/D and f_{osc} for d/D=1.43 (a-column) and d/D=4.00 (b-column)

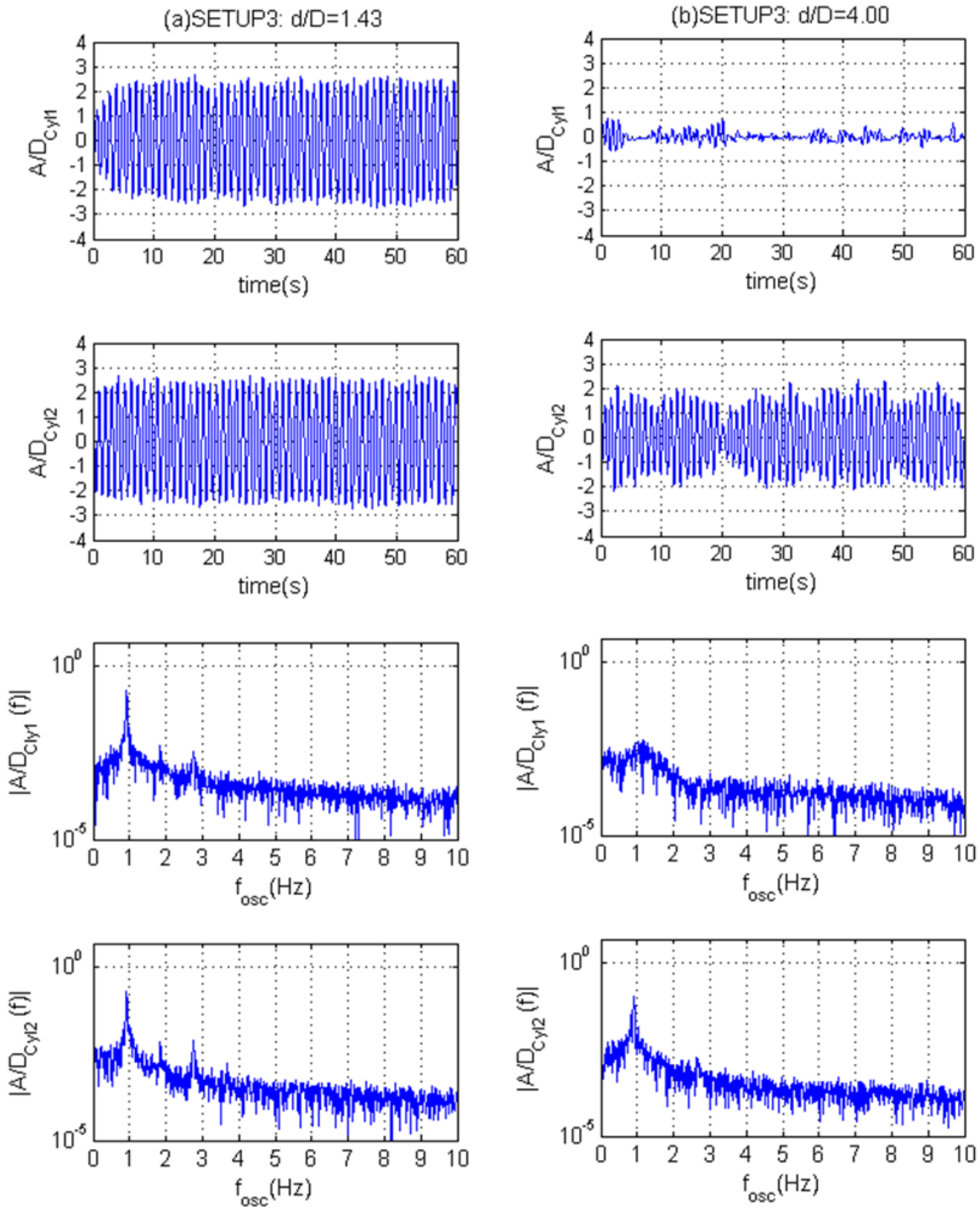

Figure 7.23: U^*=11.78 (Re=72,700); A/D and f_{osc} for d/D=1.43 (a-column) and d/D=4.00 (b-column)

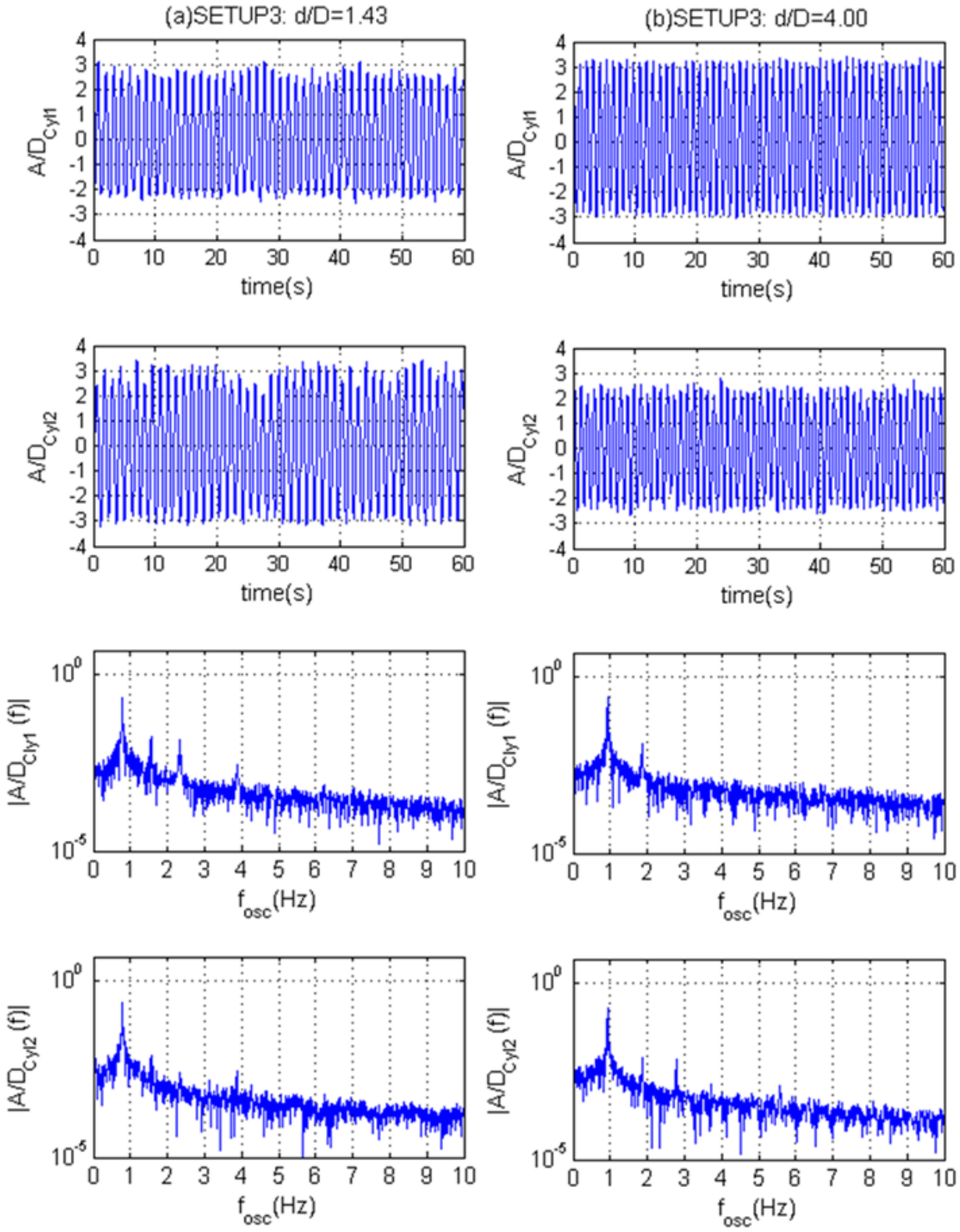

Figure 7.24: U^*=15.25 (Re=94,000); A/D and f_{osc} for d/D=1.43 (a-column) and d/D=4.00 (b-column)

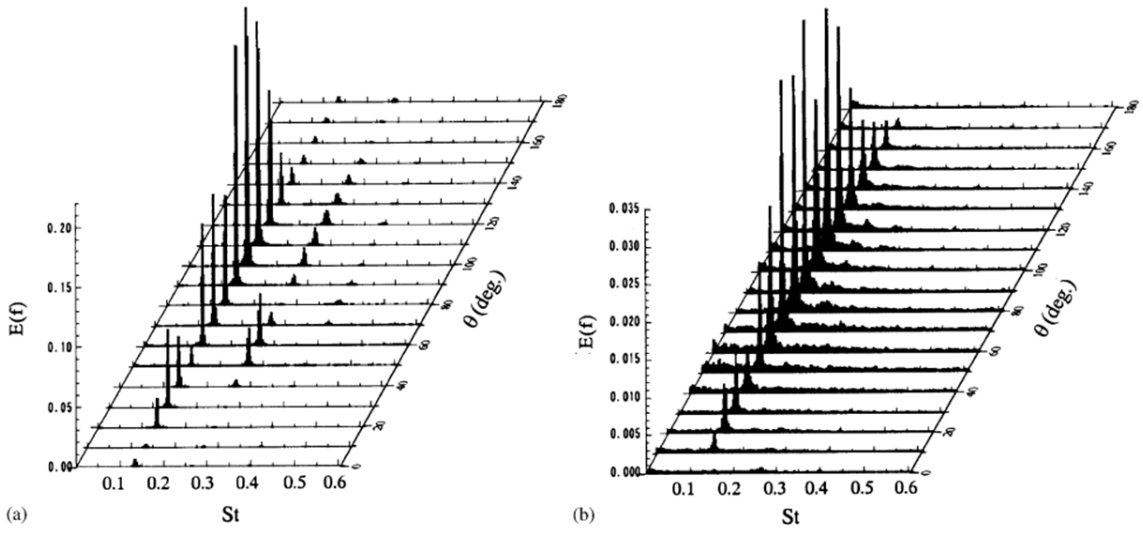

Figure 7.25: Power spectrum distribution obtained from fluctuation in pressure on the surface of the downstream cylinder; (a) d/D=1.40 and (b) d/D=2.50 [Reproduced from Alam et al., 2003a]

- For d/D=1.43 and 4.0, the A/D of the 1^{st} cylinder is 0.818 and 0.847, respectively and only one major frequency appears in the plot.

- For the 2^{nd} cylinders, the A/D beats for both spacing values due to the effect of two different FIMs. Two major frequencies are shown up in the frequency plot for both spacings. One is the frequency of the upstream vortex shedding and the other is the frequency of the downstream vortex shedding. The frequency of the upstream vortex shedding is still dominant

Figure 7.22: U^*=9.89 (Re=60,800)

- This is in the TrSL3 region and almost the end of the upper branch of VIV.

- For d/D=1.43, both up and downstream cylinders show the beating phenomenon and in their frequency plots, both have two major frequencies but the beating is caused by different reasons for the up and downstream cylinders. For the upstream cylinder, the beating is caused by the transition from VIV to galloping

while the downstream cylinder beats due to the effects of its own VIV and the upstream wake.

- Frequency of the downstream vortex shedding is dominant in the frequency plots of downstream cylinders for both setups.
- For d/D=4, the upstream cylinder is still in VIV and A/D is almost sinusoidal.

Figure 7.23: U^*=11.78 (Re=72,700)

- This is at the end of the transition region from VIV to galloping.
- For d/D=1.43, both the upstream and the downstream cylinders are in galloping. A/D is almost sinusoidal and only one major frequency appears near its natural frequency in the water and two super harmonic frequencies also show up. The downstream cylinder oscillates independently and not much affected by the upstream wake. The A/D of both cylinders are 2.4.
- For d/D=4.0, the oscillation of the upstream cylinder is unstable and no major frequency is shown in its frequency plot. This is the end of the lower branch of VIV. This region is clearly separated from the galloping region. As shown in Figure 7.12, as the distance between upstream and downstream cylinders diminishes, the separation gap becomes smaller and disappears when d/D is smaller than 2. The downstream cylinder still shows the beats because it is also in the transition region to galloping.

Figure 7.24: U^*=15.25 (Re=94,000)

- This is in the fully developed galloping region for all cylinders and oscillations of all cylinders are almost sinusoidal and independently.
- For d/D=1.43, A/D of the upstream and downstream cylinders is 2.89 and 3.07, respectively. The downstream cylinder has higher oscillatory amplitude.

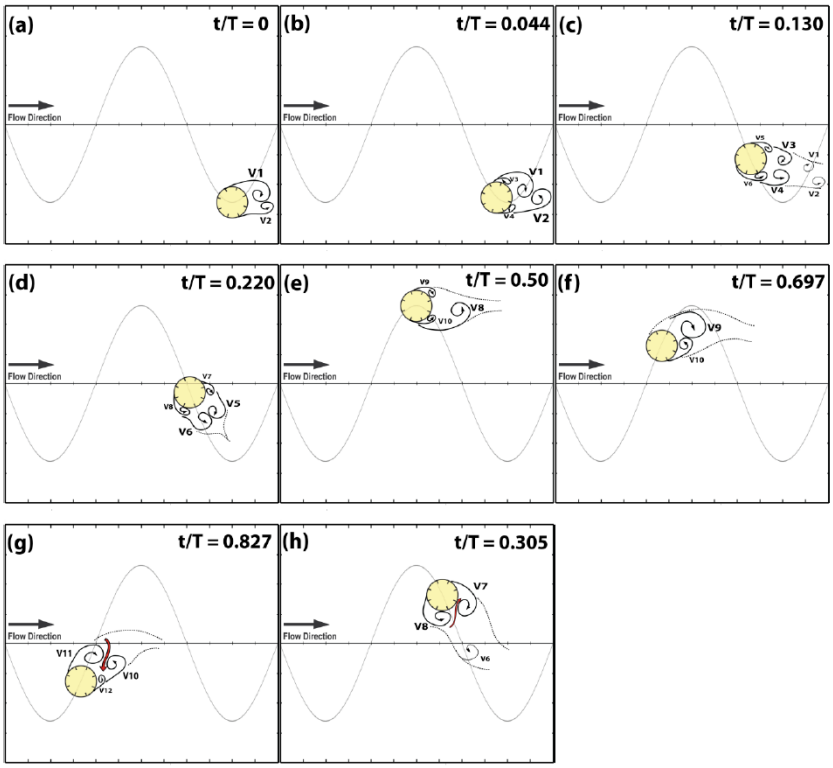

Figure 7.26: Flow structure of a single cylinder with PTC at U^*=11.53 (Galloping branch) [Reproduced from Chang, 2010]

- For d/D=4.0, the A/D of the up and downstream cylinders are 3.24 and 2.68.
- Many super harmonic frequencies appear in all frequency plots. This is because of high number of vortices shedding. Chang(2010) investigated the vortex shedding mode of a single cylinder with PTC in galloping by visualization and observed that a total of 10 vortices shed per cylinder of oscillation at U^*=11.53 as shown in Figure 7.26.

7.3.3 Effect of mass ratio

The effect of the mass ratio on a single cylinder in VIV were discussed in Section 5.1.1. Previous observations (Khalak and Williamson, 1997b, 1999; Govardhan and Williamson, 2002; Williamson and Govardhan, 2004) show that lower mass ratio broaden the upper branch with higher oscillatory amplitude and for the critical mass

ratio of 0.52, VIV oscillations never stop (Govardhan and Williamson, 2002). These investigations were all for a single smooth cylinder in VIV at low Reynolds numbers. There is, however, no investigation of the effect of the mass ratio on two circular cylinders with PTC in galloping to the best of the authors' knowledge. In this section, the effect of the mass ratio on FIMs of two cylinders with PTC in tandem arrangement is studied experimentally with three different mass ratios. Additional mass plates made of brass were attached at both ends of the cylinders to increase the oscillatory mass and there by the mass ratio as shown Figure 7.16.

Figure 7.27: Additional mass attached at the end of the two cylinders

7.3.3.1 Experimental setup

Details of the experimental setups are described in Table 7.3. All experiments were conducted in the Reynolds number (Re=UD/ν) range of 36,000 102,000. The spring stiffness and damping ratio were kept as close as possible in the tests.

7.3.3.2 Results and discussion

The results of the Setup 5 are compared to those of the Setup 7. From this section to next section, comparisons are made among three systems with different properties in the same graph. Therefore, the dimensionless quantity, U^*, cannot be used as an

Table 7.3: Details of experimental conditions

SETUP 6	*m* (kg)	*k* (N/m)	*C* (Ns/m)	*m**	*ζ*	*fn,w*
1st Device	7.861	770.10	3.981	1.344	0.0256	1.219
2nd Device	7.858	771.72	3.624	1.341	0.0233	1.220
			Parameter			
d/D		1.43			2.00	
SETUP 7	*m* (kg)	*k* (N/m)	*C* (Ns/m)	*m**	*ζ*	*fn,w*
1st Device	3.470	737.46	3.241	0.650	0.0321	1.462
2nd Device	3.475	736.69	2.935	0.651	0.0290	1.461
			Parameter			
d/D		1.43			2.00	

independent variable because it depends on the system's spring and mass parameters. Instead, Reynolds number is used to plot the figures for comparison.

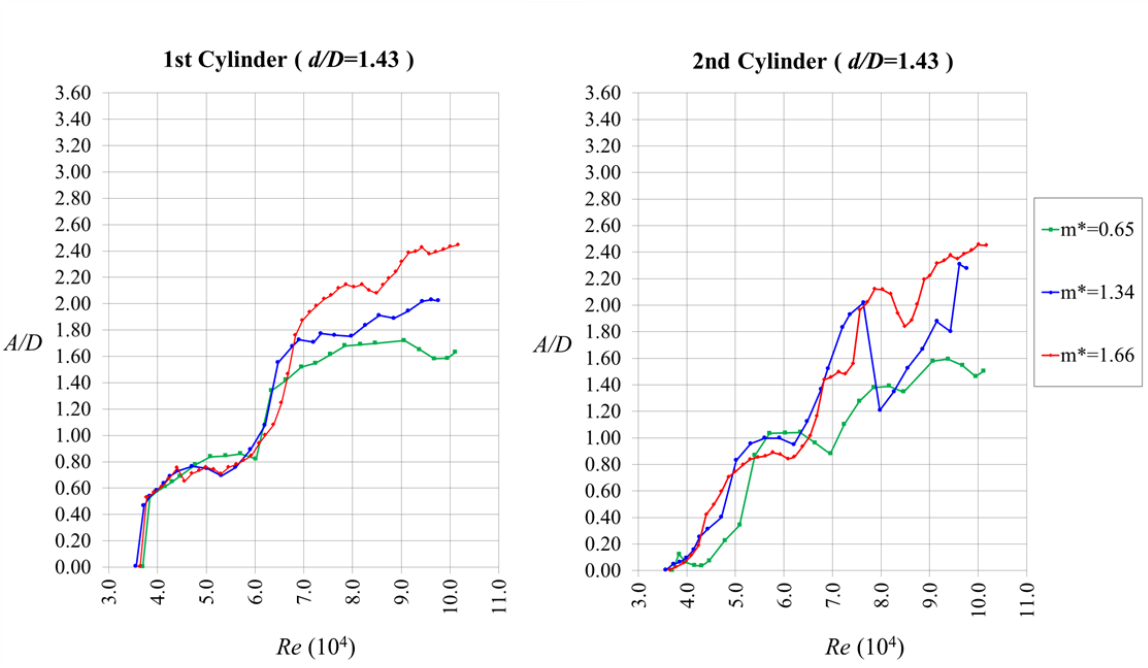

Figure 7.28: Effect of the mass ratio on A/D of two cylinders with PTC - d/D=1.43 - Setup 5 to 7

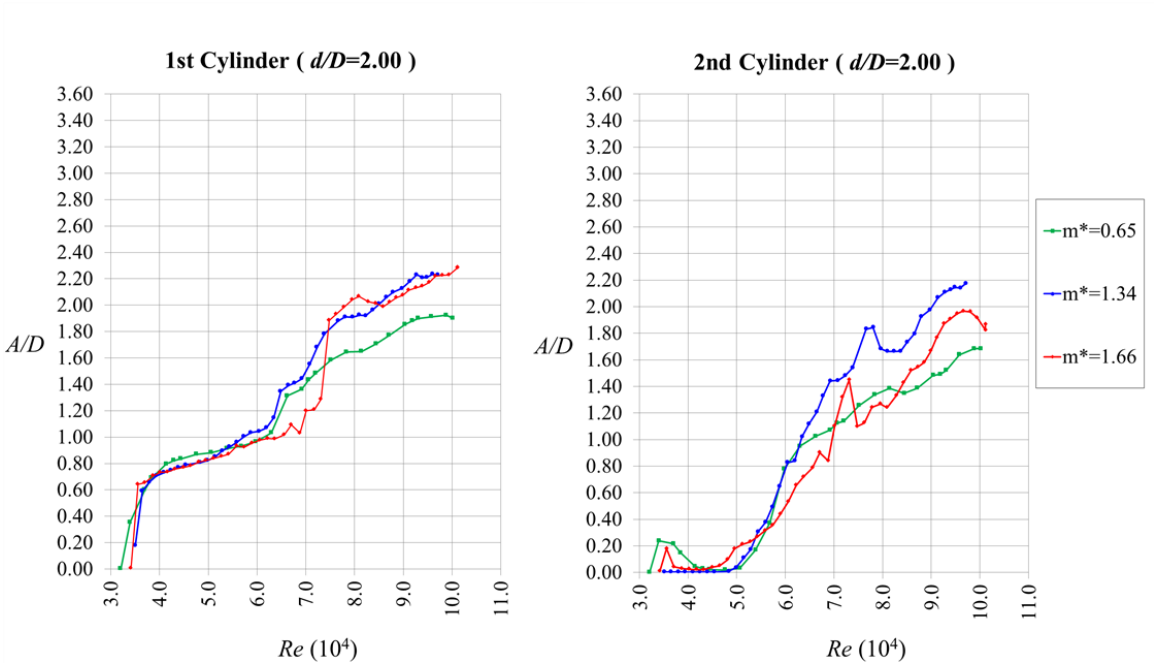

Figure 7.29: Effect of the mass ratio on A/D of two cylinders with PTC - d/D=2.00 - Setup 5 to 7

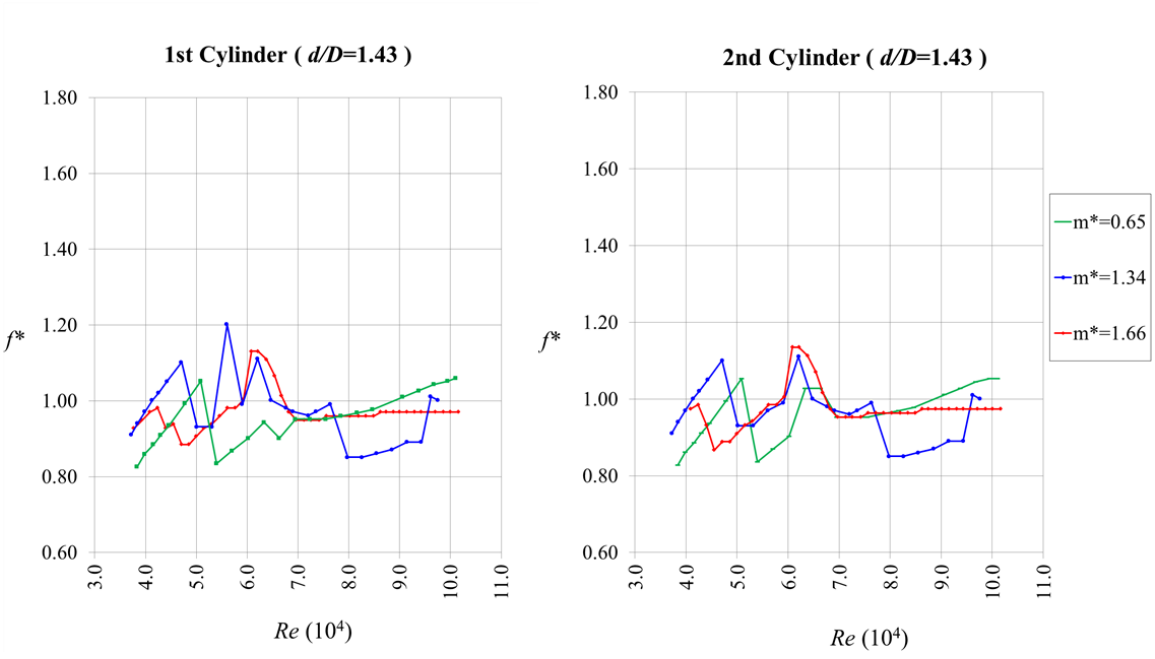

Figure 7.30: Effect of mass ratio on f^* of two cylinders with PTC - d/D = 1.43 - Setup 5 to 7

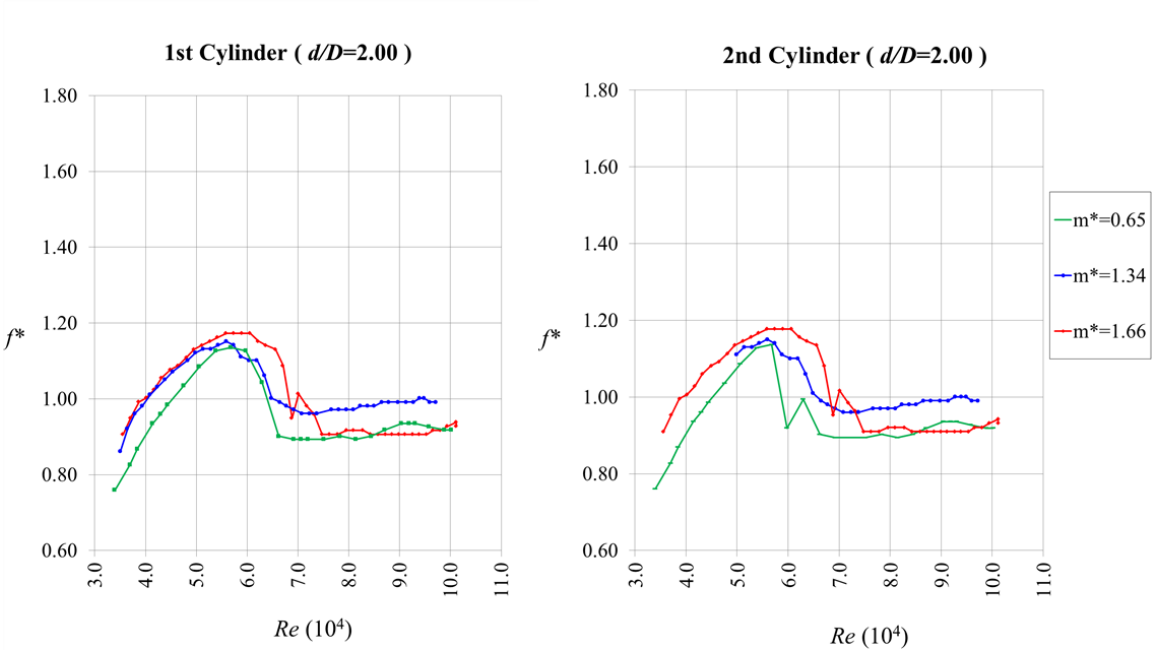

Figure 7.31: Effect of mass ratio on f^* of two cylinders with PTC - d/D=2.00 - Setup 5 to 7

$A/D$and f^* of the 1^{st} cylinders: Figures 7.28 to 7.31

- The effects of high mass ratio is different between VIV and galloping regions.
- As previously observed by other researchers (Khalak and Williamson, 1997b, 1999; Govardhan and Williamson, 2002; Williamson and Govardhan, 2004), in the VIV region, the maximum A/D increases and the upper branch becomes wider as the mass ratio decreases. The difference of the maximum A/D between m*=0.65 and 1.66 is 5% 8% in VIV.
- However, as the mass ratio increases, the A/D of the 1^{st} cylinder in galloping increases. The difference of the maximum A/D between m*=0.65 and 1.66 is 15.8% for d/D=2.0 and it is 29.7% for d/D=1.43.
- For d/D=1.43, the oscillatory frequency fluctuates due to the strong interference between the 1^{st} and 2^{nd} cylinder and it is difficult to find a trend.

- For d/D=2.0, the frequency ratio is higher for higher mass ratio in the VIV region and it is 0.92 for m*=0.65 and 1.66 but for m*=1.34, it is 0.99 in galloping.

***A/D*and f^* of the 2^{nd} cylinders: Figures 7.28 to 7.31**

- For d/D=1.43, the maximum A/D increases with decrease in the mass ratio before galloping region but it increases with increase in the mass ratio in the fully galloped region. The A/D in galloping shows fluctuation.
- For d/D=2.0, the upper branch of the 2^{nd} cylinder was suppressed and the A/D in galloping doesn't show a trend. The A/D of two high mass ratios are still higher than that of the lowest mass ratio.
- For d/D=1.43, the frequency plot doesn't show any trend.
- For d/D=2.0, the frequency response shows the same trend found in the 1^{st} cylinder.

7.3.4 Effect of spring stiffness

The effect of spring stiffness is studied experimentally with three different spring stiffness values. For comparison, results of three previous setups of tests, Setup 3, Setup 4, and Setup 7 are plotted in Figures 7.21to 7.24.

***A/D*and f^* of the 1^{st} cylinder: Figures 7.32 to 7.35**

- VIV starts at lower Re and the synchronization region broaden as the spring stiffness decreases.
- The maximum A/D in VIV isn't influenced by the spring stiffness.
- For U^*=525N/m, the galloping is initiated earlier than other spring stiffness.
- The A/D in fully galloped region increases with decrease in spring stiffness.

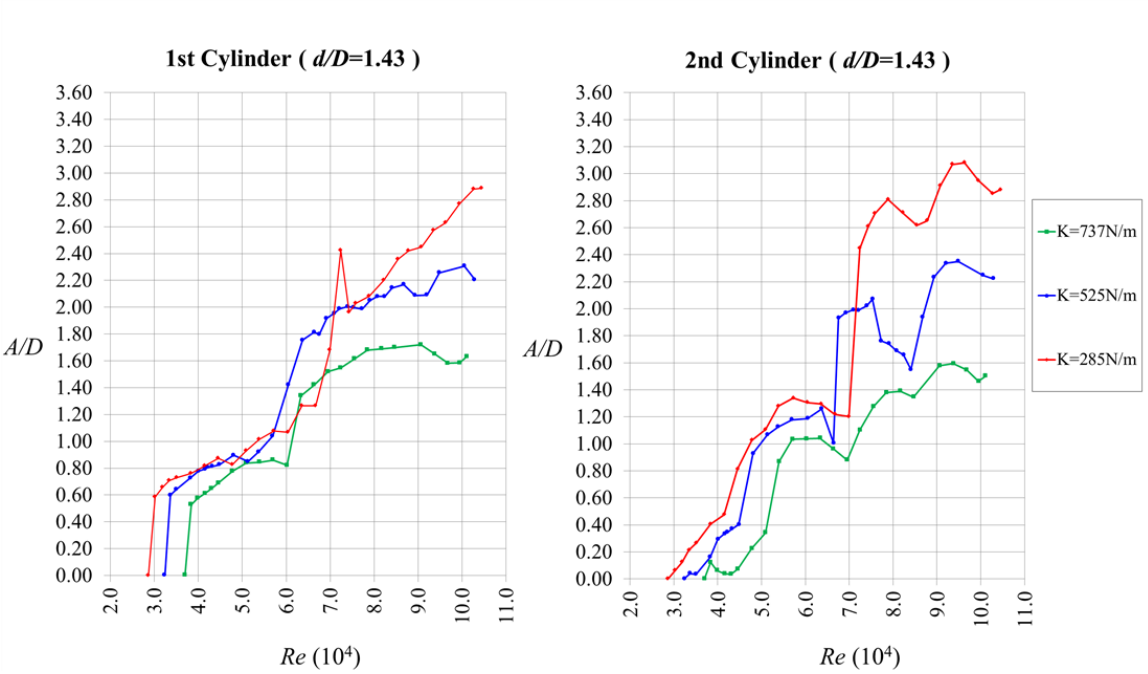

Figure 7.32: Effect of spring stiffness on A/D of two cylinders with PTC - d/D=1.43

- The oscillatory frequency ratio is higher for lower spring stiffness and it is reversed in the fully galloped region.

$A/D$and f^* of the 2^{st} cylinder: Figures 7.32 to 7.35

- A/D is higher for the softer spring in most of the regions.
- Galloping is initiated at lower Re as the spring stiffness decreases.
- The oscillatory frequency ratios fluctuate in the transition region of the 1^{st} cylinder from VIV to galloping.
- The trend in the frequency ratio plot is very similar to that of the 1^{st} cylinder.

7.4 Main Findings

Several observations were made based on the test results throughout this chapter. The major findings are summarized below.

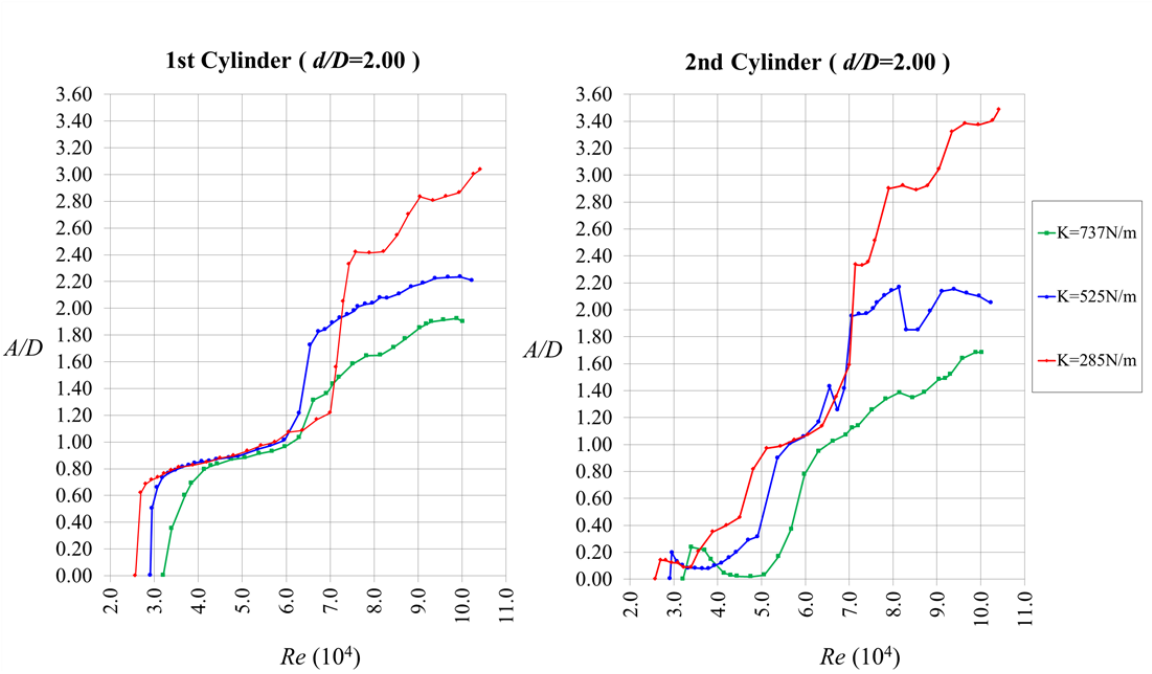

Figure 7.33: Effect of spring stiffness on A/D of two cylinders with PTC - d/D=2.00

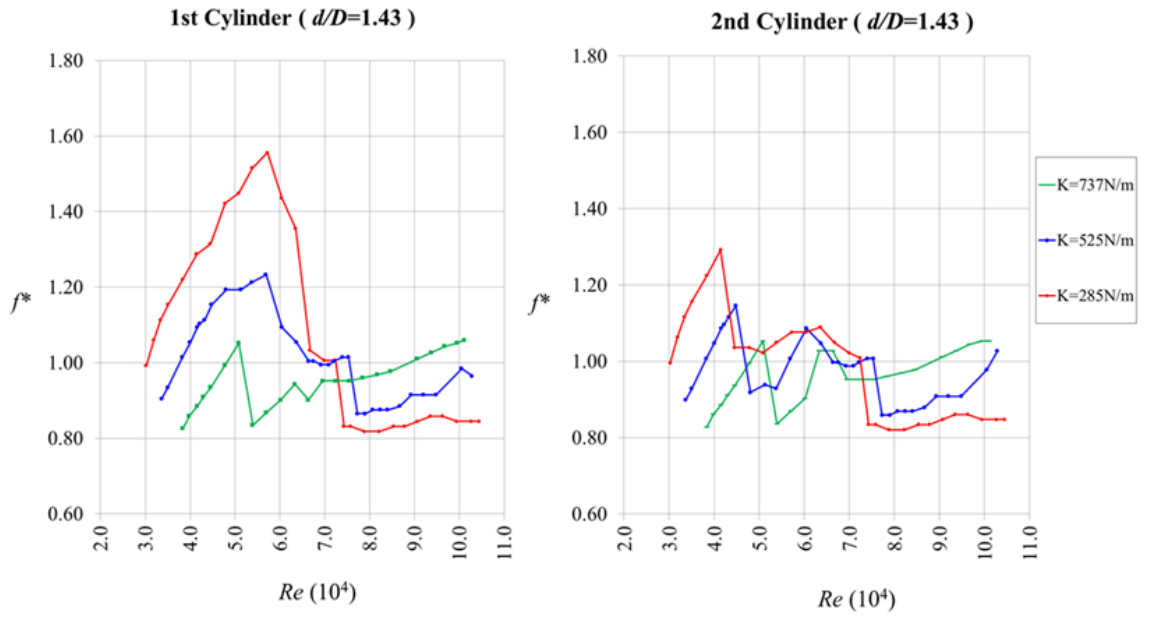

Figure 7.34: Effect of spring stiffness on f^* of two cylinders with PTC - d/D=1.43

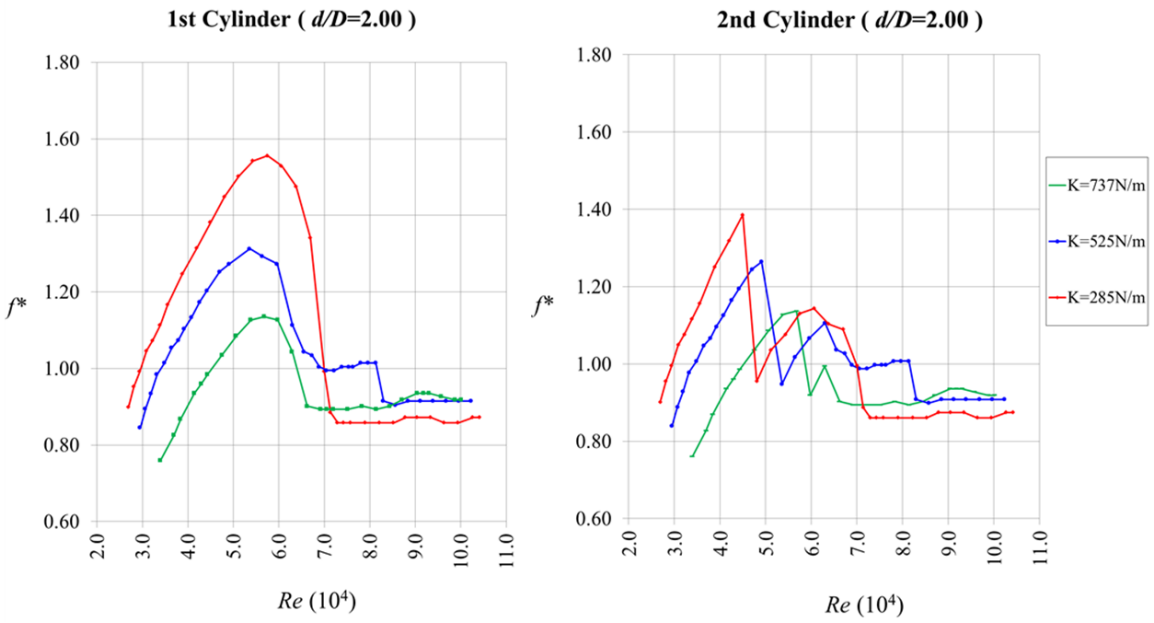

Figure 7.35: Effect of spring stiffness on f^* of two cylinders with PTC - d/D=2.00

FIM of two smooth cylinders in tandem arrangement

- The A/D results were in good agreement with the measurements in Chapter 4. The 1^{st} cylinder was not affected by the presence of the 2^{nd} cylinder and the A/D response of the 1^{st} cylinder for $d/D \geq 2.57$ followed the single cylinder response. For d/D=2.0, the trend of the amplitude response deviates compared to the previous results in Chapter 4 due to the effect of the spring stiffness. This discrepancy became smaller with increase in the spring stiffness. The oscillation frequency of the 1^{st} cylinder in tandem arrangement was slightly higher than that of the single cylinder for most tandem spacings excepted for d/D=1.43.

- The trend of response of the 2^{nd} cylinder was very different from the results of the 1^{st} cylinder. For $d/D \geq 2.57$, the oscillatory amplitude in the upper branch was suppressed and the maximum A/D and synchronization region decreased with increasing in the tandem spacing. The A/D bump was observed in the region of $4.5 < U^* < 7$. This might be due to the change of vortex shedding

mode in the upstream cylinder.(Laneville and Brike, 1999).

- For d/D=1.43, the amplitude and frequency response of both the 1^{st} and 2^{nd} cylinder were very different from those of other spacings due to the effect of the strong wake interference between the two cylinders. The upper branch of the 1^{st} cylinder was suppressed while in the lower branch, the 1^{st} cylinder kept oscillating with almost constant amplitude of $1.2D$ until the flow speed reached the maximum allowable limit of the LTFSW Channel.

- For d/D=1.43, the amplitude of 2^{nd} cylinder reached a maximum value of $1.2D$ for both spring stiffness values, and this value is two times higher compared to that of other spacings. Strong beating phenomenon was observed in the amplitude time history plots of both the 1^{st} and the 2^{nd} cylinders in the region of $6.0< U^* <9.0$. For the smallest spacing values, the oscillation frequencies of both the 1^{st} and the 2^{nd} cylinders were clearly lower than that of other spacing values.

FIM of Two Cylinders with PTC

- Both cylinders with the PTC achieved back-to-back VIV and galloping regardless of the tandem spacings, mass ratio, and spring stiffness.

- The dynamic response of both cylinders with PTC in tandem arrangement were distinguished by the tandem spacing of d/D=2.0. For $d/D\geq$2.0, the amplitude response of the 1^{st} cylinder was not significantly affected by the presence of the downstream cylinder while for d/D=1.43, the amplitude of the 1^{st} cylinder in galloping was much lower compared with that of other tandem spacing values.

- For d/D=1.43, the amplitude of the 2^{nd} cylinder with the PTC was significantly higher for most reduced velocities compared with that for other tandem spacings. The discrepancy increased with increasing spring stiffness.

- For d/D=1.43 and 2.0, the frequency response of both the 1^{st} and the 2^{nd} cylinders with PTC was relatively low compared with that of other spacings for most reduced velocities.

- The effects of high mass ratio was different between VIV and galloping regions. The maximum amplitude of both the 1^{st} and the 2^{nd} cylinders in VIV region slightly increased with decreasing the mass ratio, where the amplitude was higher for the higher mass ratio in the galloping region.

- The amplitude responses of both cylinders in galloping were considerately influenced by the spring stiffness and the maximum amplitude increased as the spring stiffness decreased. For K=285N/m and d/D=2.0, the amplitudes of the 1^{st} and the 2^{nd} cylinders at $U^* = 17$ reached $3.04D$ and $3.49D$, respectively.

CHAPTER VIII

ENERGY CONVERSION

In this chapter, the effects of parameters such as the tandem spacing, staggering, PTC, mass ratio, spring stiffness, and number of cylinders on the energy conversion from hydrokinetic in the flow to mechanical in VIVACE are studied. The hydrokinetic energy in the flow is converted to the mechanical energy in VIVACE by the interference between the flow and the cylinders. In previous studies on a single cylinder VIVACE (Lee and Bernitsas, 2011; Lee et al. 2011; Chang and Bernitsas, 2011) the energy conversion of a single cylinder VIVACE was presented in terms of the total mechanical power. The total mechanical power is defined as the work done by the fluid force per time period T and given by

$$P_{mech} = \frac{1}{T}\int_0^T F_{fluid,Total}(t)\dot{y}\,\mathrm{d}t \tag{8.1}$$

where $F_{fluid,Total}$ is the total time dependent transverse fluid force acting on an oscillating cylinder in the transverse direction of the flow. The equation of motion of the cylinder oscillating transversely to the flow is given by

$$m_{osc}\ddot{y} + c_{mech}\dot{y} + Ky = F_{fluid,Total}(t) \tag{8.2}$$

where m_{osc}, c_{mech}, and K are the mass of the oscillating parts, total mechanical

damping coefficient, and spring stiffness. The mechanical damping is a linear sum of the structural damping, c_{sys}, and the harness damping, $c_{harness}$, that is an additional linear viscous damping is introduced in to the system to harness power from the flow. Thus, the mechanical damping is given as

$$c_{mech} = c_{sys} + c_{harness} \tag{8.3}$$

Substituting Eqn. (8.2) into Eqn. (8.1)), the power equation can be rewritten as

$$P_{mech} = \frac{1}{T}\int_0^T \left(m_{osc}\ddot{y} + (c_{sys} + c_{harness})\dot{y} + Ky\right)\dot{y}\,\mathrm{d}t \tag{8.4}$$

The dynamic response of the cylinder of VIVACE in VIV or galloping can be assumed as a sinusoidal oscillation. By this assumption, the only nonzero term in Eqn. (8.4) is the velocity-square dependent term and thus by subtracting the Eqn. (8.3) for the Eqn. (8.4), the equation can be rewritten and divided into two components, which are the harnessed power due to the harness damping and the dissipated power due to the structural damping, as follows

$$P_{harness} = \frac{1}{T}\int_0^T c_{harness}\dot{y}^2\,\mathrm{d}t \tag{8.5}$$

$$P_{diss} = \frac{1}{T}\int_0^T c_{sys}\dot{y}^2\,\mathrm{d}t \tag{8.6}$$

In previous studies on a single cylinder VIVACE (Lee and Bernitsas, 2011; Lee et al. 2011; Chang and Bernitsas, 2011), the harnessed power was obtained by introducing the additional harness damping into the VIVACE system by using the virtual damper-spring (Vck) system. The Vck system replaced the real damper and real springs of the VIVACE system by a servo-motor and electric control system. Further

details of the Vck system can be found in the paper by Lee et al. (2011).

The V_{ck} system for a multiple-cylinder VIVACE is still in development, and thus the additional harness damping couldn't be introduced in the multiple-cylinders VIVACE system, and only the real spring-damper system was used for all experiments in this dissertation. Therefore, the energy conversion cannot be measured because the total mechanical power calculated by using Eqn. (8.4) presents only the dissipated power due to the structural damping.

In order to evaluate, however, the effect of the various parameters on the energy conversion, a quantitative comparison in terms of energy between the test results should be conducted. For that purpose, the total converted energy, E_{Mech}, is introduced and defined as

$$E_{Mech} = \frac{1}{2}KA^2 + \int_0^T c_{sys}\dot{y}^2 \, \mathrm{d}t \tag{8.7}$$

where A is the amplitude of the oscillation. On the right hand side of Eqn. (8.7), the first term accounts for the total mechanical energy of the VIVACE system in VIV or galloping where the amplitude response has been assumed to be sinusoidal, and the second term is the work done by the structural damping per cycle.

Assuming that the sinusoidal oscillation has a constant amplitude A, the equation can be rewritten as

$$\begin{aligned} E_{Mech} &= \frac{1}{2}KA^2 + \int_0^T c_{sys} \left(2\pi f A \cos(2\pi f t)\right)^2 \, \mathrm{d}t \\ &= \frac{1}{2}KA^2 + 2c_{sys}\pi^2 f^2 A^2 \end{aligned} \tag{8.8}$$

where f is the oscillation frequency.

It should be emphasized that the concept of the total converted energy could not be theoretically accurate but it is still useful to present the effects of the parameters on

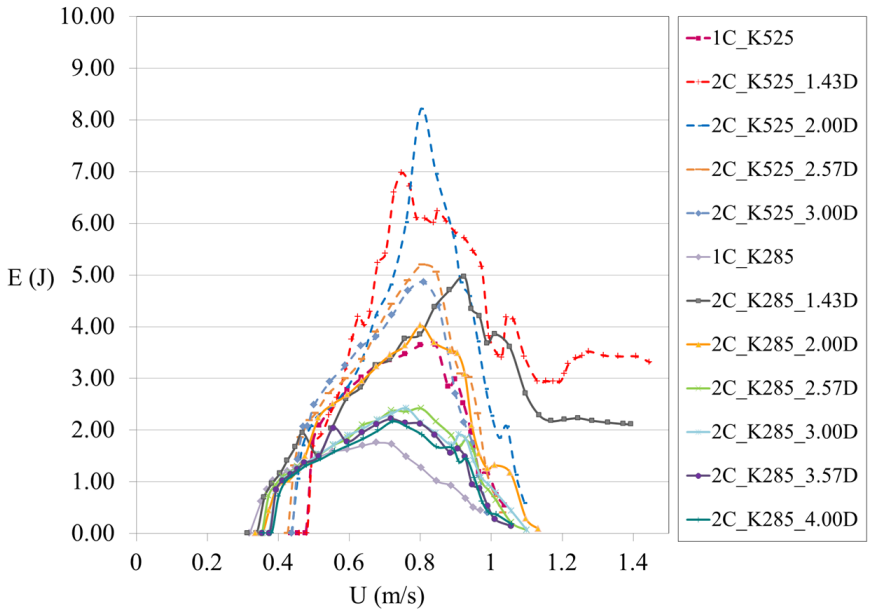

Figure 8.1: Total converted energy by two smooth-cylinders VIVACE Converter with different tandem spacing and spring stiffness

the energy conversion from the flow to the multiple-cylinders VIVACE system. It can be justified though based on free oscillation tests conducted in water. Those showed that the mechanical power stored in the springs by an initial static displacement in the free oscillation test is dissipated in less than a cycle.

8.1 Energy Conversion by Two-Smooth-Cylinders VIVACE Converter

Figure 8.1 shows the total converted energy by two smooth VIVACE cylinders calculated based on the results presented in Section 7.3. The designations of # C, K000, and 000D indicate the number of cylinders, spring stiffness in N/m, and the center-to-center spacing between two cylinders in tandem.

a. The total converted energy for the two cylinders VIVACE increases with decreasing the spacing between the two cylinders in tandem.

b. For d/D=1.43D and 2.00D, the total converted energy for the two cylinders

VIVACE is much higher than that of larger spacing.

c. The total converted energy for the two cylinders VIVACE is almost equal with that for the one cylinder VIVACE in the region of the flow speed lower than 0.6m/s because the oscillation of the downstream cylinder is very small in that region.

d. Most peaks of the total converted energy for both the one-cylinder and two-cylinder VIVACE occurs in the region of $0.7 < U < 0.85$m/s.

e. For d/D=1.43, the two-cylinders VIVACE can harness energy in the region of $U > 1.0$.

f. For both spring stiffness values, the largest total converted energy for the two cylinders VIVACE is shown at 0.8m/s for the spacing of $2.0D$.

g. The total converted energy for both the one-cylinder and the two-cylinders VIVACE increases with increasing the spring stiffness at most of the flow speed.

h. Based on the test results, for the two-smooth cylinder VIVACE, the best configuration of the center-to-center spacing and spring stiffness to achieve the highest total converted energy is $2.0D$ and 525N/m.

8.2 Effect of PTC on Energy Conversion by Two-Cylinders VIVACE Converter

In order to investigate the effect of the PTC on the total converted energy for the two-cylinder VIVACE, the experimental data for two center-to-center spacing values in Sections 4.1 and 4.2 are used. The total converted energy of the two-cylinder VIVACE with the PTC are calculated for three different configurations of the PTCs, and results are compared with those of the two smooth-cylinder VIVACE converter.

In Figures 8.2 and 8.3, the legend related to P60:$\alpha-\beta$ indicates that sandpaper with roughness P60 is attached starting at α degrees symmetrically on both side of the upstream cylinder and at β degrees symmetrically on both side of the downstream cylinder. The following conclusions can be drawn:

a. The total converted energy for the two cylinders with the PTC is significantly increased compared with that of the total converted energy for the two cylinders without the PTC.

b. For d/D=2.0, the total converted energy for the two cylinders with PTC reaches up to 53.8J at U=1.337m/s regardless of the position of the PTC while 18.4J is the highest value for two cylinder without the PTC at U=1.05m/s.

c. For d/D=2.0, in the region of $0.58<U<0.86$m/s, the total converted energy for the two cylinders without the PTC has slightly higher value than that for the two cylinders with the PTC. For d/D=2.5, the region is $0.58<U<0.98$m/s, and the different between the total converted energy for two cylinder with the PTC and without the PTC is larger.

d. For d/D=2.0, the total converted energy with the PTC configuration of P60:20-30 shows slightly higher values in most of the flow speeds than those for other PTC configurations. A similar trend is shown for d/D=2.5 but the values are fluctuating in the galloping region, and the maximum value of 54.5J is achieved at 1.337m/s for the PTC configuration of P60:30-30.

e. For both spacing values, P60:20-30 is the best choice among three PTC configurations for $U<1.12$m/s in terms of the total converted energy except for the case of no PTC. In the galloping region, the PTC configuration does not significantly influence the energy conversion.

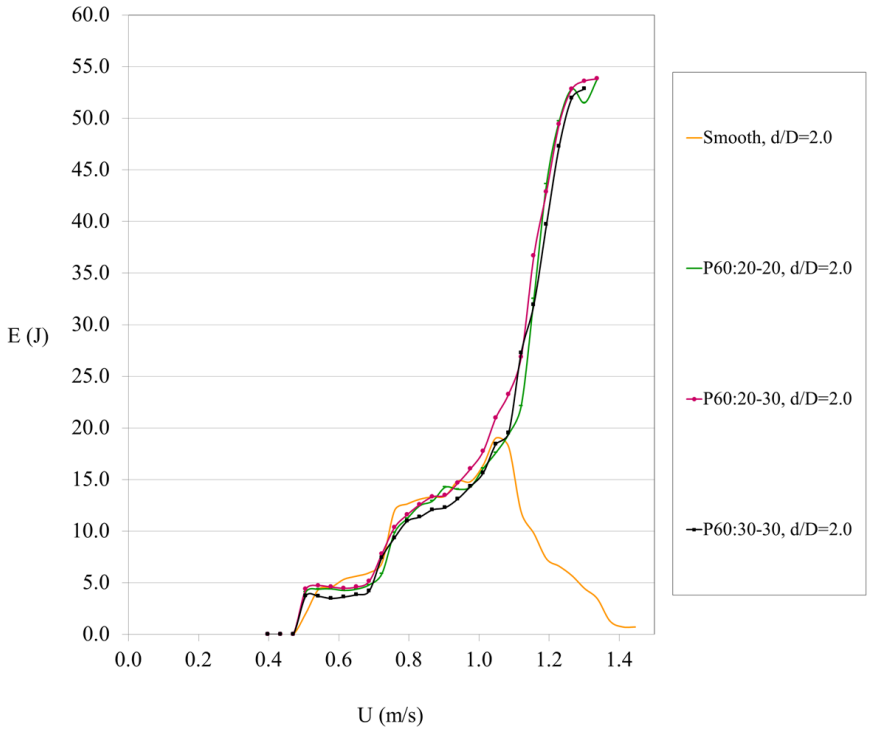

Figure 8.2: Effect of PTC on total converted energy by two-cylinders VIVACE Converter for d/D=2.5 and K=745N/m: data from Sections 4.1 and 4.2

8.3 Effect of Mass Ratio on Energy Conversion by Two-PTC-Cylinders VIVACE Converter

Based on the experimental data from Section 7.4.2, the total converted energy by a two-cylinder VIVACE converter with PTC for three different mass ratios was calculated and compared with each other. For comparison, two tandem spacing values of d/D=1.43 and 2.00 were selected because for these two spacing, the total converted energy is higher than that of other spacing values. The results are plotted in Figure 8.4.

a. The total converted energy considerably increases as the mass ratio increases in the region of U>0.89m/s.

b. For d/D=1.43 and m^*=1.66, the total converted energy is considerably higher than that of other cases, and it reaches its maximum value of 50.8J at U=1.33m/s

while the maximum value is 21.57J at 1.20m/s for d/D=1.43 and m^*=0.65.

c. In the region of 0.45<U<0.89m/s, the differences in the total converted energy among the three mass ratios are small. It is the contrary result to the expectation which the lower mass ratio could increase the energy conversion by achieving higher amplitude than the higher mass ratio does. In fact, the amplitude was slightly higher for the lower mass ratio in the VIV region as shown in Figures 7.28 and 7.29, but it is compensated by the mass in the calculation of the total converted energy.

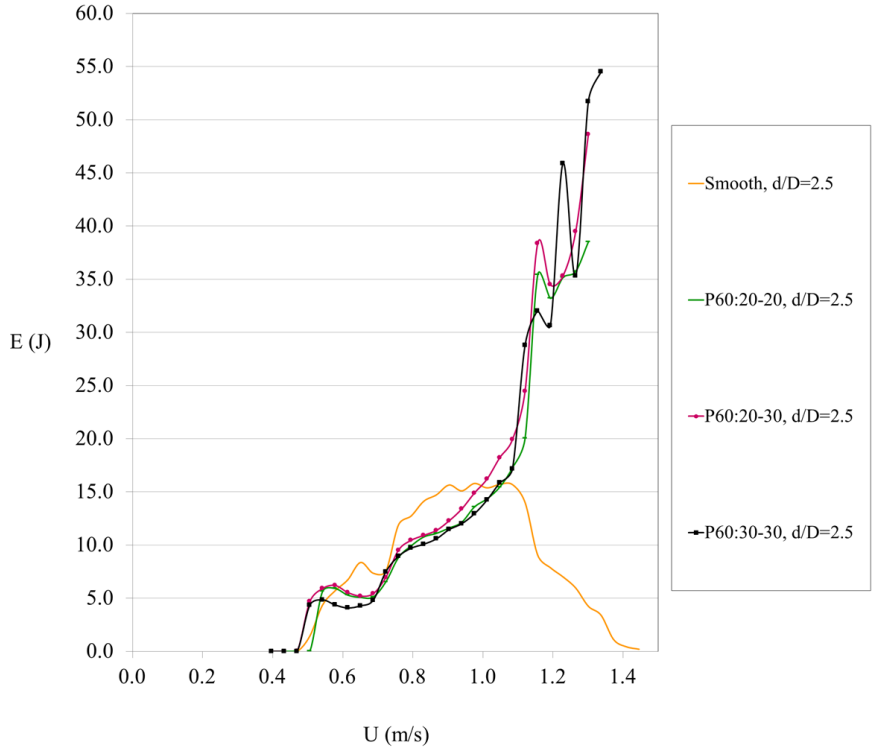

Figure 8.3: Effect of PTC on total converted energy by two-cylinders VIVACE Converter for d/D=2.5 and K=745N/m: data from Sections 4.1 and 4.2

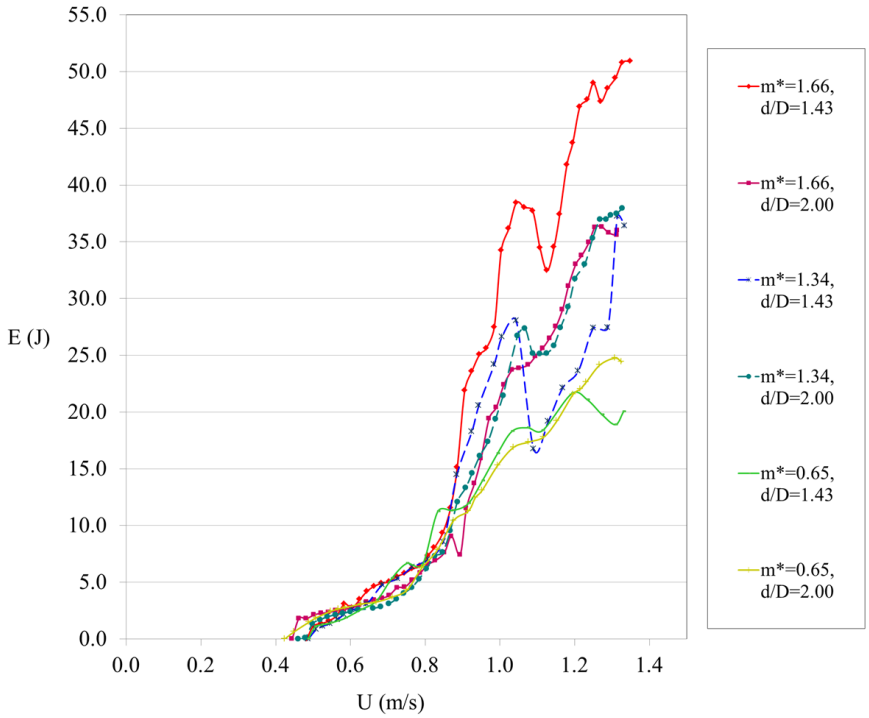

Figure 8.4: Effect of mass ratio on total converted energy by two-PTC-cylinders VIVACE Converter for d/D=1.43 and 2.0, and K=737−800N/m: data from Section 7.4.2

8.4 Effect of Spring Stiffness on Energy Conversion by Two-PTC-Cylinders VIVACE Converter

The effect of the spring stiffness on the total converted energy of two cylinders VIVACE with the PTC is studied. The plot was produced from the experimental data in Section 7.4.3.

a. The total converted energy is higher for the stiffer spring in the VIV region as previously noticed in Section 8.1. In the fully developed galloping region, the trend is reversed for d/D=2.0 because the amplitude increases with decreasing the spring stiffness and the total converted energy is proportional to the amplitude-square while it linearly increases with increasing the spring stiffness.

b. As the spring stiffness increases, the total converted energy is generally higher in

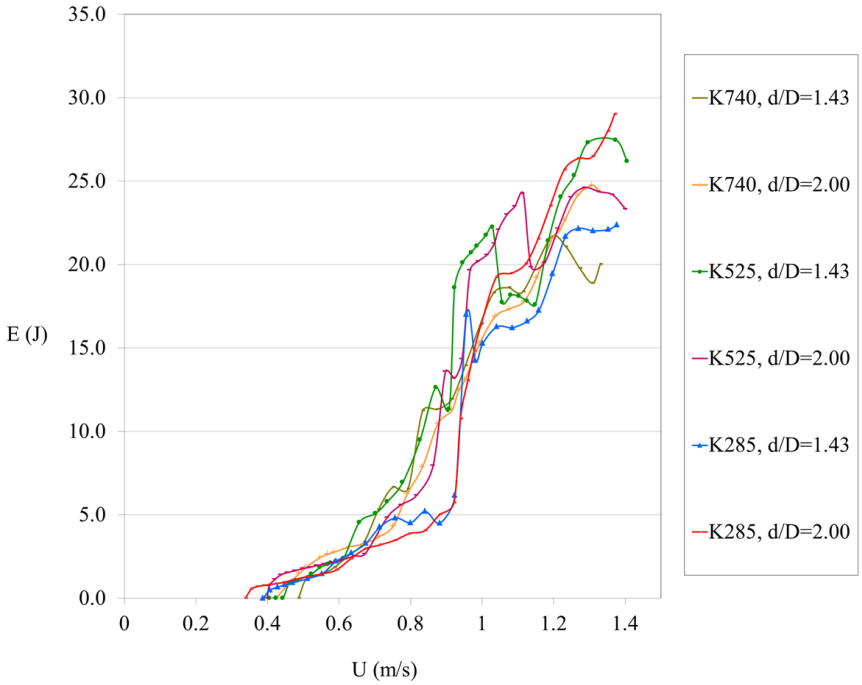

Figure 8.5: Effect of spring stiffness on total converted energy by two-PTC-cylinders VIVACE Converter for d/D=1.43 and 2.0, and m^*≈0.64: data from Section 7.4.3

the region of 0.65$<U<$0.87m/s. But for K=525N/m, the total converted energy suddenly jumps at U=0.95m/s and it is considerably higher than that of other cases until it suddenly drops at U=1.04m/s for d/D=1.43 and at U=1.11m/s for d/D=2.0.

8.5 Effect of Tandem Spacing on Energy Conversion by Multiple-PTC-Cylinders VIVACE Converter

In this section, the effect of the tandem spacing on the total converted energy for two, three, and four-cylinder VIVACE with PTC is investigated. Figure 8.6 are plotted based on the data produced from the 3^{rd} generation of the two-cylinder VIVACE in Section 7.4.2. In Figure 8.7, the plot was generated by the data of the 2^{nd} generation two-cylinder VIVACE in Section 4.3. For Figures 8.8 and 8.9, the

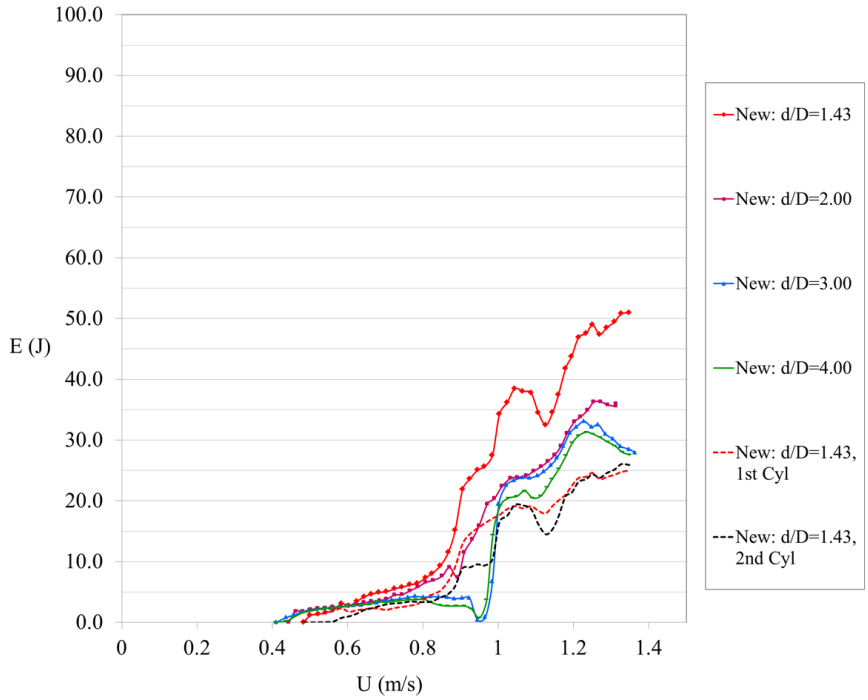

Figure 8.6: Effect of tandem spacing on total converted energy by two-PTC-cylinders VIVACE Converter for K=800N/m and m^* ≈1.66: data from Section 7.4.2

data of three and four-cylinders VIVACE in Section 4.5 were used to produce the plots. In each figure, the total converted energy of each cylinder was plotted to see the contribution to the total converted energy for the multiple-cylinder VIVACE converters. The designation of Old and New indicates the 2^{nd} generation VIVACE and the 3^{rd} generation VIVACE, respectively. In all figures, the legend related to #'st Cyl. indicates the sequence number of a cylinder from upstream.

Figure 8.6: Two cylinders with PTC: 3^{rd} generation of VIVACE

a. The total converted energy increases with decreasing tandem spacing in most of the flow speeds. Particularly, for d/D=1.43, the total converted energy is considerably higher in the region of U>0.9m/s.

b. Compared to the results of the 2^{nd} generation devices, the total converted energy of the 3^{rd} generation is much lower in the galloped region (U >1.1m/s) for

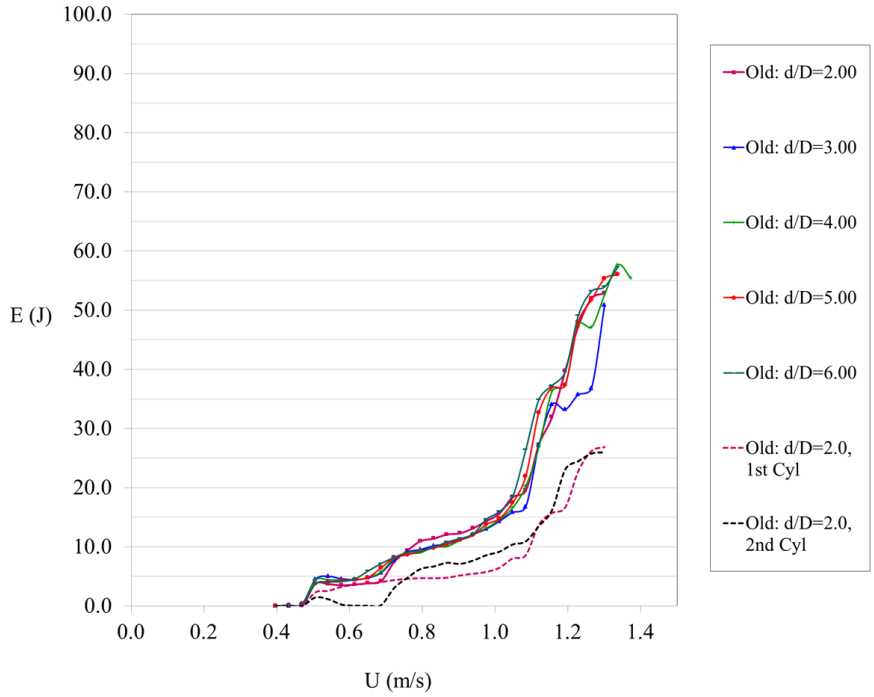

Figure 8.7: Effect of tandem spacing on total converted energy by two-PTC-cylinders VIVACE Converter for $K \approx 745$N/m and $m^* \approx 1.68$: data from Section 4.3

d/D=2.0. This seems to be the resistance from the additional mass on the outside of the cylinder.

c. Each cylinder almost equally contributes to the total converted energy of the two cylinders for d/D=1.43.

Figure 8.7: Two cylinders with PTC: the 2rd generation of VIVACE

a. The tandem spacing slightly influences the total converted energy except for d/D=3.0.

b. For all tandem spacing values, the total converted energy reaches 52.7-57.0J at U=1.30m/s.

c. The converted energy for each cylinder was plotted in a dashed line. For d/D=2.0, the contribution of the upstream cylinder on the total converted

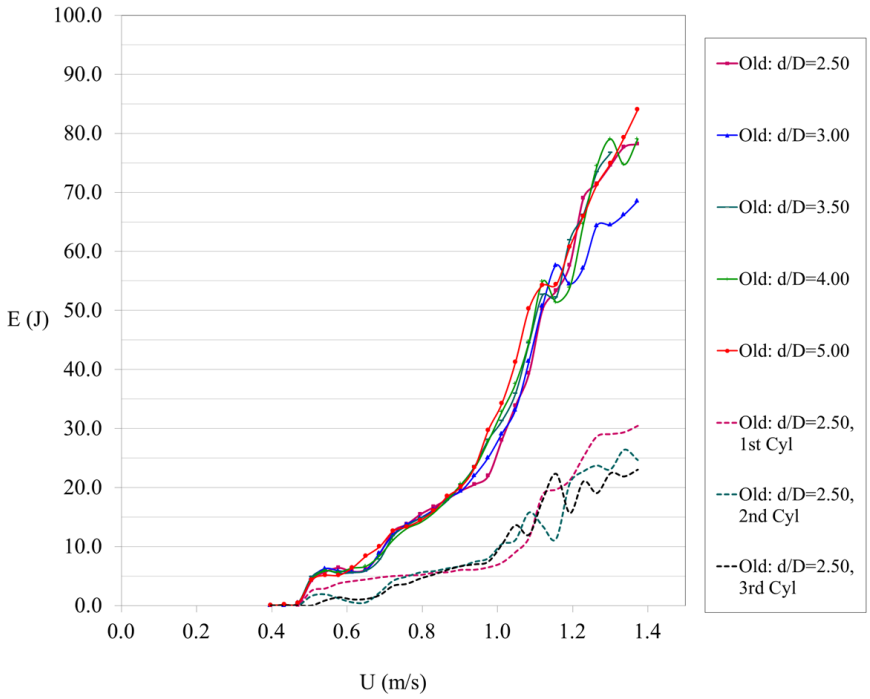

Figure 8.8: Effect of tandem spacing on total converted energy by three-PTC-cylinders VIVACE Converter for $K \approx 745$N/m and $m^* \approx 1.68$: data from Section 4.5

energy is higher in the region of $U < 0.76$m/s but in the region of $U > 0.76$m/s, the downstream cylinder contributes more or almost equally to the total energy.

Figure 8.8: Three cylinders with PTC: the 2rd generation of VIVACE

a. The total converted energy increases as the tandem spacing increases in the region of $0.94 < U < 1.12$m/s but in the remaining region, the effect of the tandem spacing is not significant.

b. For all tandem spacings except for $d/D = 3.0$, the value of the total converted energy reaches 79-84.0J at $U = 1.37$m/s.

c. The contribution of the upstream cylinder on the total converted energy is dominant in the region of $U < 0.72$m/s, each cylinder almost equally contributes on generation of the converted energy in the region of $0.72 < U < 0.97$m/s, and in the

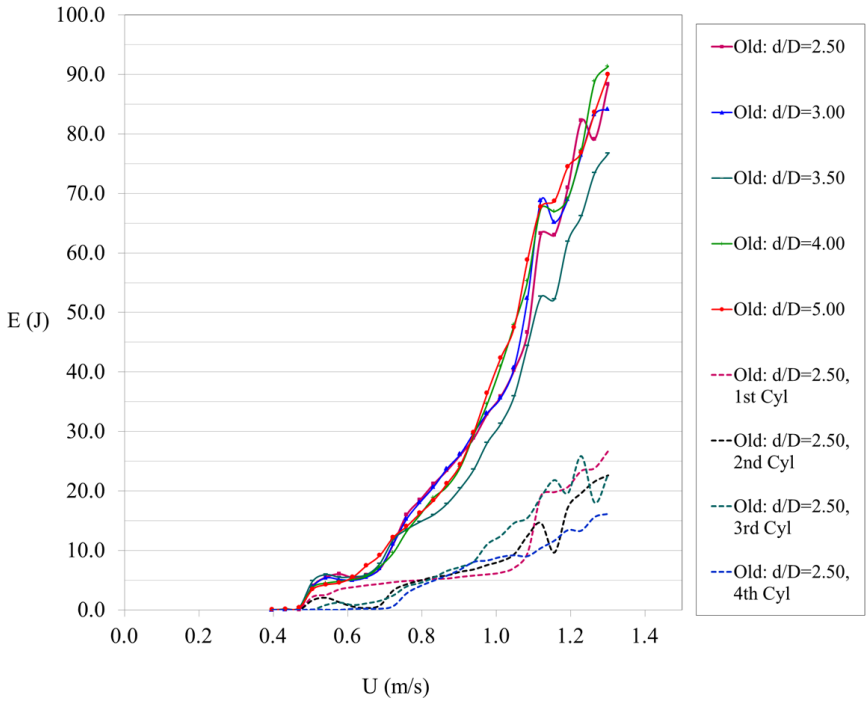

Figure 8.9: Effect of tandem spacing on total converted energy by four-PTC-cylinders VIVACE Converter for $K \approx 745$N/m and $m^* \approx 1.68$: data from Section 4.5

region of $U > 1.19$m/s, the contribution is lower for further downstream cylinder. It is because the free surface significantly decreases toward downstream and thus the amplitude of the downstream cylinders is limited by the lower free surface.

Figure 8.9: Four cylinders with PTC: the 2rd generation of VIVACE

a. As shown in Figures 8.7 to 8.9, for the tandem spacing d/D=3.0 or 3.5, the total converted energy is relatively low. This tandem spacing can be the critical spacing for the wake induced vibration in which the fluctuating lift force decreases as illustrated in Figure 2.17.

b. For all tandem spacings except for d/D=3.5, the value of the total converted energy reaches 84-90.0J at U=1.30m/s.

c. The contribution of each cylinder on the total converted energy shows the very

similar trend of the three cylinders. The contribution of the fourth cylinder is lower than that of upstream cylinders due to the effect of the free surface.

8.6 Effect of Staggering on Energy Conversion by Multiple-PTC-Cylinders VIVACE Converter

The total converted energy is calculated based on the data presented in Section 4.4 and the results were plotted in Figure 8.10. To investigate the effect of staggering on the total converted energy, the results of three different vertical spacings are compared at three different tandem spacing.

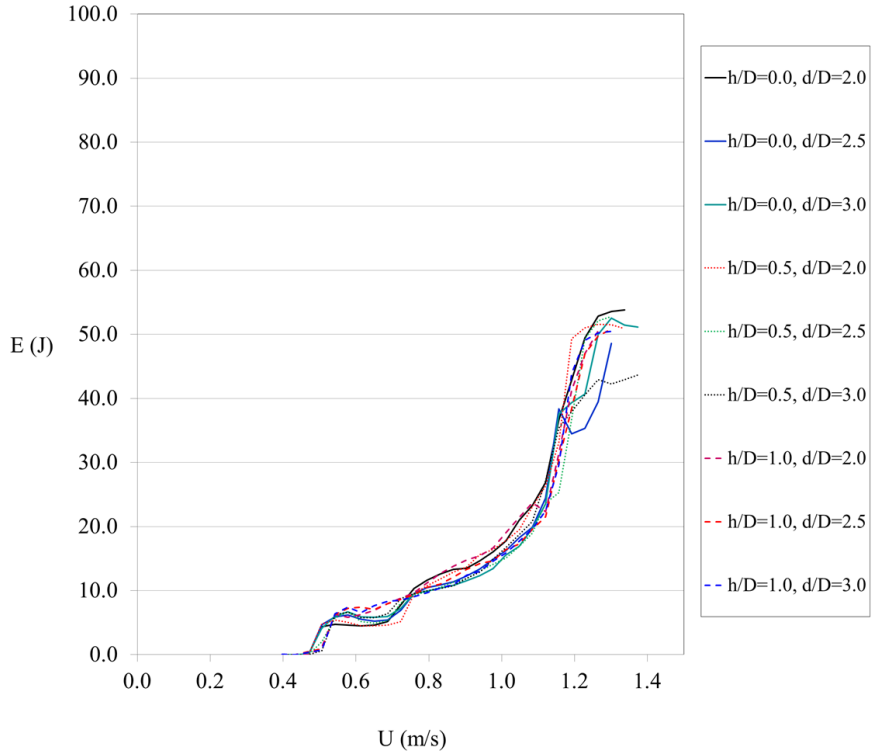

Figure 8.10: Effect of staggering on total converted energy by two-PTC-cylinders VIVACE Converter for $K \approx 745$N/m and $m^* \approx 1.68$: data from Section 4.4

a. The effect of staggering on the total converted energy is not significant.

b. As the staggering increases, the total converted energy increases for the same tandem spacing in the region of $0.58 < U < 1.12$m/s.

c. In the region of $U > 1.12$m/s, the total converted energy of the two staggered cylinders is lower. This is because the amplitude was limited by both the device and the free surface. For example, for $h/D = 1.0$, the positions of the upstream and downstream cylinders was raised and lowered by $0.5D$, respectively, and thus the maximum allowable amplitude decreased by $0.5D$ and the upstream cylinder was more likely subjected to the effect of the free surface.

8.7 Synergy of Multiple Cylinders for Hydrokinetic Energy Harnessing

Lastly, the synergy of multiple cylinders on the total energy conversion is evaluated. The total converted energy was calculated for one, two, three, and four cylinders, and compared in Figure 8.11. For this comparison, all multiple cylinders were in tandem arrangement with $d/D = 2.5$ which is the smallest tandem spacing for the three and four cylinder tests, the roughness P60 was attached starting at 30 degrees symmetrically on both sides of all cylinders, the spring stiffness was kept close to 740N/m, and the damping coefficient was in the range of $2.667 < c_{sys} < 3.464$. As shown in Figure 8.11(a), the total converted energy increases with the number of cylinders. The latter is an obvious result. Figure 8.11(b) shows more notable results. The total converted energy of a single cylinder very slightly increases with increasing the flow velocity in the VIV region. In that region, for multiple cylinders, the total converted energy gradually increases. As discussed earlier, the amplitude of the downstream cylinders in WIV is greater than that of the 1^{st} cylinder. As a result, the total converted energy normalized by the value of the single cylinder is greater than the number of cylinders in the region of $0.8 < U < 1.12$m/s as shown in Figure 8.11(b).

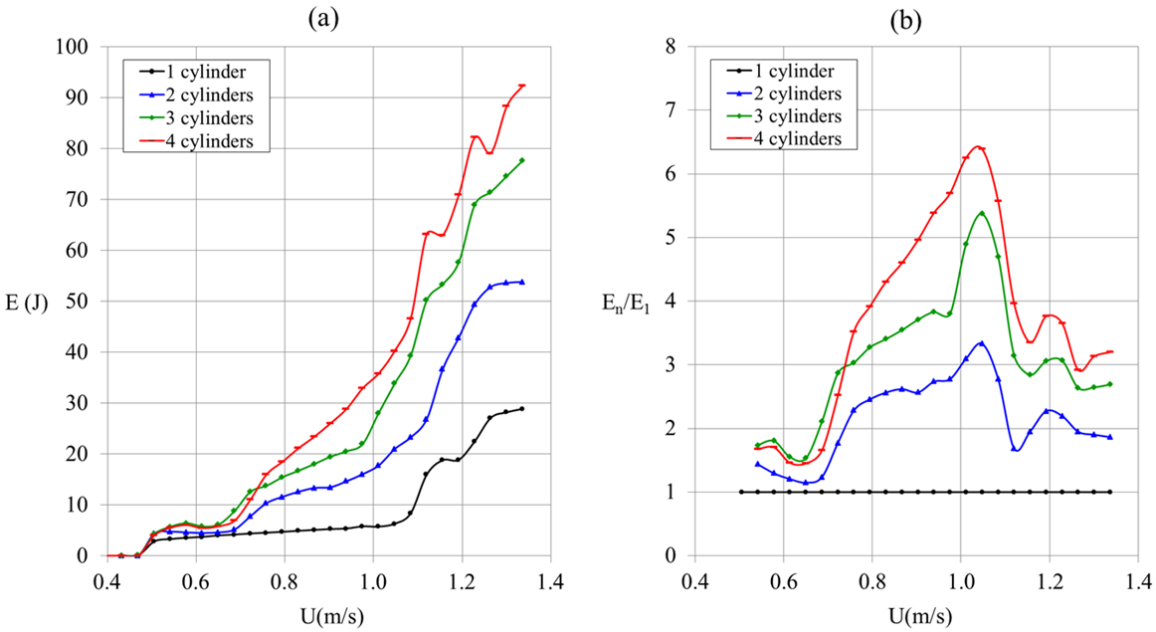

Figure 8.11: Synergy of multiple cylinders on total energy conversion: (a) total converted energy and (b) normalized total converted energy as a function of free stream velocity

For instance, the normalized total converted energy of the four cylinders reaches 6.38 at U=1.08m/s, which is 1.6 times larger than the number of cylinders. This means that the synergy of multiple cylinders on harnessing energy can be greater than the sum of the energy converted by each cylinder acting in isolation. Moreover, this is achieved for the smallest tandem spacing of $2.5D$ for the three and four cylinder tests, which indicates that the energy volume density can be increased compared with the estimation of the previous works (Lee and Bernitsas, 2011; Lee et al. 2011; Chang and Bernitsas, 2011).

In the previous estimation of power volume density (Lee and Bernitsas, 2011 ; Lee et al. 2011; Chang and Bernitsas, 2011), a staggered configuration was selected and the longitudinal distance between two cylinders was $4.0D$. Therefore, the total converted energy of two cylinders normalized by the total converted energy for d/D=4.0 and the results are shown in Figure 8.12. The results show that the normalized to-

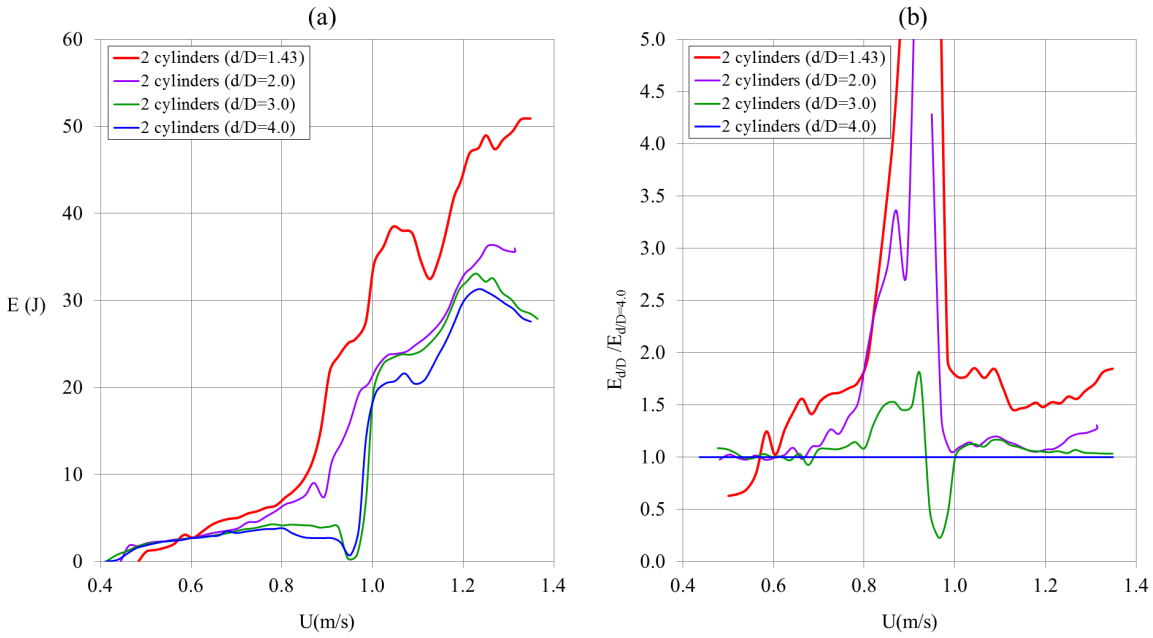

Figure 8.12: Total energy conversion for two cylinders at different tandem spacings as a function of free stream velocity: (a) total converted energy and (b) normalized total converted energy by the total converted energy at d/D=4.0

tal converted energy of two cylinders VIVACE Converter increase as the longitudinal spacing decreases. Particularly, for d/D=1.4, the normalized total converted energy is greater than 1.5 in the region of U>0.66m/s, even in the galloping region, and reaches a maximum value of 8.12 (the region of 0.91<U<0.97m/s was excluded in the comparison). This clearly indicates that the energy volume density of multiple-cylinder VIVACE Converters can be increased significantly from the previous estimation (Lee and Bernitsas, 2011; Lee et al. 2011; Chang and Bernitsas, 2011).

Based on this research, it can be concluded that a multiple-cylinder VIVACE Converter can harness more energy than the same number of cylinders acting in isolation.

CHAPTER IX

CONCLUSIONS AND RECOMMENDATIONS FOR FUTURE WORK

9.1 Conclusions

The goal of this research was to maximize the synergy of multiple parallel cylinders in Fluid Induce Motion (FIM) for hydrokinetic energy harnessing. In order to achieve this goal, the effects of tandem spacing, staggering, Passive Turbulence Control (PTC), mass ratio, spring stiffness, damping, and number of cylinders on FIM of multiple cylinders were experimentally studied. For these experimental studies, two different generations of VIVACE converters were designed and built. At the same time, the old Low Turbulence Free Surface Water (LTFSW) Channel was replaced by the new LTFSW Channel, allowing for higher amplitudes of oscillation. Based on the test facility, this dissertation is divided into two parts: Part A and Part B.

In Part A, all tests were conducted with the 2^{nd} generation of VIVACE in the old LTFSW Chanel described in Chapter 3, and with high Reynolds numbers in the range of 28,000<Re<120,000 which primarily covers the TrSL2 and TrSL3 regimes. As discussed in Chapter 4, up to four of the 2^{nd} generation devices were used to study FIM of multiple cylinders, which all were identical cylindrical tubes with diameter D=3.5" and length L=36". In this study, the variable parameters were the tandem

spacing, staggering, PTC, and number of cylinders. Results from this study brought to light the fact that by introducing the PTC all four cylinders can achieve back-to-back VIV and galloping regardless of the tandem spacing and staggering. In the galloping region, all four cylinders oscillated like pistons in a reciprocating engine and reached maximum amplitude of $2.2D$-$2.8D$ which was the limit of the old LTFSW Channel.

The 2^{nd} generation of VIVACE had many advantages such as a simple structure and motion mechanism, as well as easy setup and use. There was, however, a critical drawback to investigate galloping instability since the oscillatory amplitude of VIVACE was limited to about $3D$. The oscillatory amplitude was also restricted by the depth of the LTFSW Channel. In order to overcome the limitations of the facilities and, thus, to further investigate FIM, the 3^{rd} generation VIVACE and the new LTFSW Channel were designed and built.

In Part B, the design process of the 3^{rd} generation of VIVACE was discussed in Chapter 5, and the flow calibration process and results were presented in Chapter 6. The results of flow calibration of the new channel showed that the velocity distribution of the flow is highly symmetric and nearly uniform across the test section. In Chapter 7, FIM of multiple cylinders was further investigated with two 3^{rd} generation of VIVACE cylinders in the new LTFSW Channel. In this investigation, the variable parameters were the tandem spacing, PTC, mass ratio, and spring stiffness and tests were conducted in the range of 28,000$\leq$ Re$\leq$120,000. The smallest tandem spacing was $1.43D$ while it was $2.0D$ in the tests in Chapter 4. For this smallest spacing, both smooth and roughened cylinders exhibited distinct response with higher amplitude and lower oscillation frequency compared with those of other spacings. The effect of the mass ratio was notable. The amplitude of cylinders in VIV increased with decreasing the mass ratio which has been observed by many researchers. This feature was, however, reversed in the galloping region, and higher mass ratio resulted in

higher amplitude in both upstream and downstream cylinders. The spring stiffness significantly affected on the dynamic response of both upstream and downstream cylinders.

Finally, in Chapter 8, the energy conversion from horizontal hydrokinetic to mechanical in VIVACE were discussed based on measurements and observations made in this dissertation. In previous studies in the MRELab on power assessment, Lee et al. (2011[6]) and Chang and Bernitsas (2011[40]) used the Virtual damper and spring (Vck) system, which replaced real linear springs and damper by a servo-motor and an electric control system, to introduce an additional damping into the system. As a result they calculated the envelope of harnessed power of a single cylinder VIVACE. Unfortunately, the Vck system for multiple-cylinder VIVACE converters in the new LTFSW Channel and with the third generation of VIVACE converters is still under development. Thus, the harnessed power could not be measured in this research. Instead, the concept of total converted energy was introduced in order to assess the effects of the parameters studied in Chapters 4 and 7 on the energy conversion. Results of this assessment on the energy conversion reveal that the multiple-cylinder VIVACE Converters can synergistically work in close proximity to each other and considerably increase the power volume density of VIVACE Converter.

Summary of the conclusions:

a. By introducing PTC, all cylinders (2,3,4 tandem configurations) achieve galloping increasing the range of FIM synchronization with high amplitudes (2.2-3.49D) regardless of other parameters.

b. For tandem spacing of 1.43D, FIM of two cylinders in tandem is distinct: galloping starts earlier, amplitude is higher for the 2^{nd} cylinder, oscillation frequency is lower for both cylinders, and energy harnessed is 60% higher.

c. For two cylinders in close tandem proximity (d/D<2.0), contrary to single cylin-

der studies, energy envelope points in galloping may not correspond to the highest spring stiffness.

d. Higher mass ratio (m^*) results in higher marine hydro-kinetic energy conversion in galloping with practically no change in the VIV region. Increase by a factor of 2.5 was measured for $0.65<m^*<1.66$.

e. Multiple cylinders in tandem can be in synergistic FIM in close proximity of $d/D<2.0$.

f. 2, 3, and 4 cylinders in synergistic FIM can harness more marine hydro-kinetic energy than the sum of the energy harnessed by each cylinder acting in isolation.

9.2 Contributions

Summary of the contributions:

a. Effect of PTC on FIM of two cylinders: Experimental investigation and demonstration that galloping can be triggered on both cylinders by introducing PTC.

b. Effect of PTC on FIM of three cylinders: Experimental investigation and demonstration that galloping can be triggered on all three cylinders by introducing PTC.

c. Effect of PTC on FIM of four cylinders: Experimental investigation and demonstration that galloping can be triggered on all four cylinders by introducing PTC.

d. Effect of tandem spacing: Experimental demonstration that the smaller spacing enhances FIM of multiple cylinders.

e. Effect of mass ratio: Experimental demonstration that higher mass ratio enhances galloping.

f. Synergistic FIM of two cylinders can harness up to 1.6 times the MHK energy than two cylinders can harness acting in isolation.

g. Synergistic FIM of three cylinders can harness up to 1.8 times the MHK energy than three cylinders can harness acting in isolation.

h. Synergistic FIM of four cylinders can harness up to 1.6 times the MHK energy than two cylinders can harness acting in isolation.

9.3 Recommendations to Future Work

From this research we learned that FIM can be enhanced in two ways: (a) Optimizing system parameters such as the mass ratio and spring stiffness; and (b) optimizing multiple-cylinder arrangement. Even though the effect of several different configurations of parameters on FIM of multiple cylinders were studied in this research, those studies are not still enough to fully understand the effects of those parameters on FIM and determine optimal configuration and parameter combinations for hydrokinetic energy harnessing. Therefore, the following work is recommended:

a. Further investigation on tandem spacing for $d/D \leq 2.0$: As discussed in Chapter 7, the dynamic response of both upstream and downstream cylinders in this region showed promising results for hydrokinetic energy harnessing but in this dissertation only two tandem spacings were studied. Extensive study in this region will give optimal tandem spacing to maximize the power density of VIVACE.

b. Extensive study on mass ratio: Based on the results of Chapter 8, the mass ratio is a critical parameter to enhance FIM and thereby hydrokinetic energy conversion.

c. Investigate Flow Induced Motion in multiple circular cylinders with PTC using visualization: As shown in the completed research there are various kinds of FIM induced by the interference between cylinders. Investigation of the FIM in downstream cylinders is needed to understand the underlying mechanism by proper visualization method.

d. Studies on wake-boundary layer interaction: For downstream cylinders, it is expected to be a serious issue as also evident in the current research results. The boundary layers of downstream cylinders are undeniably subjected to the action of upstream cylinder wakes contributing to cylinder dynamics. But, this aspect has not been studied so far. Many features of cylinder oscillations could be made clear through this study and it is planned for the future.

e. Extending staggered configurations for increased power harnessing: In the tests conducted so far, only two h/D values were considered, viz., 0.5 and 1.0. More experiments to confirm the effect of staggered configuration on the FIM of cylinders are needed. In the new LTFSW Channel more tests on the staggered configurations at additional vertical spacing ratios should be conducted. It is expected that more vertical spacing can cause more oscillation amplitude in downstream cylinders in the range of Re<70,000. That will improve the power density of multiple-cylinder VIVACE Converters at relatively low current speed.

f. Effect of spring stiffness for improved power density: The spring stiffness in the model tests was decided randomly and was not controllable. Previous studies (Bernitsas et al. 2008, 2009) showed that power harnessing can be improved by changing the spring stiffness at different speeds of current (Lee and Bernitsas, 2011; Chang and Bernitsas 2012). However, the effect of spring stiffness in multiple cylinder VIVACE Converters has not been conducted. This will be carried out with the Vck system. Optimal spring stiffness for each device can

be derived to improve power density.

g. Effect of damping for improved power density: Damping is another important parameter, which affects both the phenomenon of FIM and performance of the VIVACE Converter. Therefore, damping should be carefully controlled to improve power density. Various damping values will be applied by the Vck system to maximize power density.

h. Power envelope for optimal power harnessing: The VIVACE Converter aims to maximize power harnessing from river or ocean currents. Its performance depends on the combination of damping and spring stiffness and speed of current besides the location and roughness of PTC. Therefore, it is important to control damping and spring stiffness at each current speed to maximize the power harnessing.

BIBLIOGRAPHY

BIBLIOGRAPHY

1. Absi, R., 2011. An ordinary differential equation for velocity distribution and dip-phenomenon in open channel flows, *Journal of Hydraulic Research*. Vol. 49. 82-89.

2. Absi, R., 2008. Comments on Turbulent velocity profile in fully-developed open channel flows. *Environ. Fluid Mech*. 8, 389–394.

3. Alam, M.M., Moriya, M., Takai, K., Sakamoto, H., 2003a. Fluctuating fluid forces acting on two circular cylinders in a tandem arrangement at a subcritical Reynolds number. *Journal of Wind Engineering and Industrial Aerodynamics* , 91, 139–154.

4. Alam, M.M., Moriya, M., Sakamoto, H., 2003b. Aerodynamic characteristics of two side-by-side circular cylinders and application of wavelet analysis on the switching phenomenon. *Journal of Fluids and Structures* 18, 325–346.

5. Alam, M. M., Sakamoto, H., and Zhou, Y., 2005. Determination of Flow Configurations and Fluid Forces Acting on Two Staggered Circular Cylinders of Equal Diameter in Cross-Flow, *Journal of Fluids and Structures*, 21, 363–394.

6. Alam, M.M., Sakamoto, H., 2005. Investigation of Strouhal frequencies of two staggered bluff bodies and detection of multistable flow by wavelets. *Journal of Fluids and Structures* 20, 425–449.

7. Alam, M.M., Zhou, Y., 2008. Strouhal numbers, forces and flow structures around two tandem cylinders of different diameters. *Journal of Fluids and Structures* 24, 505–526.

8. Alonso, G., Meseguer, J., Pérez-Grande, I., 2005. Galloping oscillations of two-dimensional triangular cross-sectional bodies *Exp. Fluids* 38, 789–795.

9. Alonso, G., Meseguer, J., Pérez-Grande, I., 2007. Galloping stability of triangular cross-sectional bodies: A systematic approach, *Journal of Wind Engineering and Industrial Aerodynamics* 95, 928–940.

10. Alonso G., Valero E., Meseguer J., 2009. An analysis on the dependence on cross section geometry of galloping instability of two dimensional bodies having either biconvex or rhomboidal cross sections. *European Journal of Mechanics B/Fluids* 28, 328-334.

11. Aquamarine Power - Wave Energy Company, Developer of Oyster Wave Power. Web. 3 May 2013. <http://www.aquamarinepower.com/>.

12. Assi, G. R. S., Meneghini, J. R., Aranha, J. A. P., Bearman, P. W., and Casaprima, E., 2006. Experimental Investigation of Flow-Induced Vibration Interference Between Two Circular Cylinders, *Journal of Fluids and Structures* 22, 819–827.

13. Assi, G. R. S., Bearman, P.W., Meneghini, J. R., 2010. On the wake-induced vibration of tandem circular cylinders: the vortex interaction excitation mechanism, *Journal of Fluid Mechanics*, 661, 365–401.

14. AWS Ocean Energy Ltd. - Ocena Power Company, Developer of Archimedes Wave Swing. Web. 3 May 2013. < http://www.awsocean.com>.

15. Bearman, P. W. 1984 Vortex shedding from oscillating bluff bodies. *Annual Review of Fluid Mechanics* 16, 195-222.

16. Bearman, P.W., 2011. Circular cylinder wakes and vortex-induced vibrations. *Journal of Fluid Mechanics* 27, 648–658.

17. Bernitsas, M. M., Ben-Simon, Y., Raghavan, K., and Garcia, E. M. H., 2006b. The VIVACE converter: Model tests at high damping and Reynolds number around 10^5, Proceedings 25th International Conference on Offshore Mechanics and Arctic Engineering-OMAE, Hamburg, Germany, 4-9 June2006; *ASME Transactions, JOMAE* Feb. 2009, Vol. 131, No. 1, 1-13.

18. Bernitsas, M. M. and Raghavan, K., May 25, 2007a. Enhancement of vortex induced forces & motion through surface roughness control, U.S. Provisional Patent Application, United States Patent and Trademark Office, Patent# 8,042,232 November 1, 2011.

19. Bernitsas, M. M. and Raghavan, K., May 25, 2007b. Reduction/suppression of vortex induced forces & motion through surface roughness control, U.S. Provisional Patent Application, United States Patent and Trademark Office *(UofM#3757)*.

20. Bernitsas, M. M., & Raghavan, K. 2008. Reduction/suppression of VIV of circular cylinders through roughness distribution at $8{,}000<Re<150{,}000\times10^5$. *Proceedings of the 27th Conference on Ocean, Offshore, and Artic Engineering*, Estoril, Portugal, June 15-20, 2008.

21. Bernitsas, M. M., Raghavan, K., Ben-Simon, Y., and Garcia, E. M. H., 2008, "VIVACE (Vortex Induced Vibration Aquatic Clean Energy): A New Concept in Generation of Clean and Renewable Energy From Fluid Flow," ASME *J. Offshore Mech. Arct. Eng.*, 130, 041101.

22. Bernitsas, M.M., Raghavan,K., 2009. Fluid motion energy converter. United States Patent and Trademark Office Patent #7, 493, 759 B2 issued on February 24, 2009.

23. Bernitsas, M.M., Ben-Simon, Y., Raghavan, K., Garcia, E.M.H., 2009. The VIVACE Converter: Model Tests at High Damping and Reynolds Number Around 100,000. *J. Offshore Mech. Arct. Eng-Trans*. ASME 131.

24. Blevins, R.D., 1990. Flow-Induced Vibration, 2nd Ed., Van Nostrand Reinhold, NY,USA.

25. Bishop, R.E.D., & Hassan, A.Y. 1964. The lift and drag forces on a circular cylinder in a flowing fluid. *Processing of the Royal Society (London), Series A* 277, 32-50.

26. Bokaian, A., and Geoola, F., 1984a. Wake-Induced Galloping of Two Interfering Circular Cylinders, *Journal of Fluid Mechanics* 146, 383–415.

27. Bokaian, A., and Geoola, F., 1984b, Proximity-Induced Galloping of Two Interfering Circular Cylinders, *Journal of Fluid Mechanics* 146, 417–449.

28. Bokaian, A. 1989. Galloping of a circular cylinder in the wake of another, *Journal of Sound and Vibration* 128, 71-85.

29. Brika, D., Laneville, A., 1999. The Flow Interaction between a stationary cylinder and a downstream flexible cylinder, *Journal of Fluids and Structures*, 13, 579-606.

30. Cardoso, A.H., Graf, W.H., Gust, G., 1989. Uniform flow in a smooth open channel. *Journal of Hydraulic Research.* 27(5), 603–616.

31. Chang, C. C., 2010. Hydrokinetic Energy Harnessing By Enhancement of Flow Induced Motion Using Passive Turbulence Control. Ph.D Thesis, Dept. of Naval Architecture & Marine Engineering, University of Michigan.

32. Chang C.C., Bernitsas M.M., 2011. Hydrokinetic energy harnessing using the VIVACE converter with passive turbulence control, Proceedings of the 30th OMAE 2011 Conf., Paper #50290, Rotterdam, The Netherlands, June 19-24, 2011.

33. Chang, C. C., Kumar, R.A., Bernitsas, M.M., 2011. VIV and galloping of single circular cylinder with surface roughness at 30,000≤ Re ≤120,000. *Ocean Engineering* 38, 1713-1732.

34. Clean Current Power System Inc., - Renewable Energy System, Developer of Tidal Turbine. Web. 3 May 2013. < http://www.cleancurrent.com>.

35. Cooper, K.R., Wardlaw, R.L., 1971. Aerodynamic instabilities in wakes. *In Proceeding of International Conference on Wind Effects on Buildings and Structures*, 647–655.

36. Chue, S.H.,1975. Pressure probes for fluid measurement. *Prog Aerospace Sci*. 16, 147–223.

37. Ding, J., Balasubramanian, S., Lokken, R., and Yung, T., 2004. Lift and damping characteristics of bare and straked cylinders at riser scale Reynolds numbers, *Proceedings of Offshore Technology Conference* Paper No. *16341*.

38. Ding, L., Bernitsas, M.M., Kim, E.S. 2013. 2-D URANS VS. Experiments of flow induced motions of two circular cylinders in tandem with passive turbulence control for 30,000<Re<105,000. *Ocean Eng.* In revision.

39. Finavera Renewables Inc. - Wind Energy Company, Developer of Aquabuoy. Web. 3 May 2013. < http://finavera.com>

40. Fox,T.A. & West, G.S. 1990. On the use of end plates with circular cylinders. *Experiments in Fluids* 9, 237-239.

41. Gartshore, I.S., 1984. Some effects of upstream turbulence on the unsteady lift forces imposed on prismatic two dimensional bodies, *ASME Journal of Fluids Engineering* 106, 418–424.

42. Govardhan R, Williamson CHK. 2000. Modes of vortex formation and frequency response for a freely-vibrating cylinder. *Journal of Fluid Mechanics* 420:85–130.

43. Govardhan, R., and Williamson, C. H. K., 2002. Resonance forever: existence of a critical mass and an infinite regime of resonance in vortex-induced vibration, *Journal of Fluid Mechanics* 473, 147-166.

44. Gracey, W., Letko, W. and RUSSELL, W. R., 1956. Wind tunnel investigations of a number of total-pressure tubes at high angles of attack—subsonic, transonic, and supersonic speeds. NACA TN 3641.

45. Gu, Z., 1996. On interference between two circular cylinders at supercritical Reynolds number. *Journal of Wind Engineering and Industrial Aerodynamics* 62, 175–190.

46. Gu, Z., Sun, T., 1999. On interference between two circular cylinders in staggered arrangement at high subcritical Reynolds numbers. *Journal of Wind Engineering and Industrial Aerodynamics* 80, 287–309.

47. Guo, J., Julien, P.Y., 2008. Application of the modified log wake law in open-channels, *Journal of Applied Fluid Mechanics* 1, 17–23.

48. Hanenkamp, W., Hammer, W., 1981. Transverse Vibration Behaviour of Cylinders In Line, *Journal of Wind Engineering and Industrial Aerodynamics*, 7, 37-53.

49. Hara, F. and Iijima, T., 1988. Vibrations of two circular cylinders in tandem subjected to two-phase bubble cross flows, *Journal of Fluids and Structure* 3, 389-404.

50. Hetz, A.A., Dhaubhadel, M. N., Telionis, D.P., 1991. Vortex shedding over five in-line cylinders, *Journal of Fluids and Structure* 5, 243-257.

51. Huer-Huarte, F.J., Bearman, P.W., 2011. Vortex and wake-induced vibrations of a tandem arrangement of two flexible circular cylinders with near wake interference, *Journal of Fluids and Structure* 27, 193-211.

52. Igarashi, T., 1981, Characteristics of the flow around two circular cylinders arranged in tandem, *Bulletin of JSME* 24, 323–331.

53. Igarashi, T., and Suzuki, K., 1984. Characteristics of the flow around three circular cylinders, *Bulletin of JSME* 27, 2397-56.

54. Igarashi, T., 1986. Characteristics of the flow around four circular cylinders Arranged in line, *Bulletin of JSME* 29, 751–757.

55. Igarashi, T., 1993. Aerodynamic Forces Acting on Three Circular Cylinders Having Different Diameters Closely Arranged in Line, *Journal of Wind Engineering and Industrial Aerodynamics* 49, 369-378.

56. Inman D. J., 2001, Engineering vibration 2nd edition, Prentice-Hall, Inc.

57. International Energy Agency, World Energy Outlook , 2012, Web. 11 April 2013. < http://www.iea.org>.

58. International Renewable Energy Agency, Renewable Power Generation Costs, 2012, Web. 11 April 2013. < http://www.irena.org>.

59. Kazakevich, M.I., Vasilenko, A.G., 1996. Closed analytical solution for galloping aeroelastic self-oscillations *Journal of Wind Engineering and Industrial Aerodynamics* 65. 353-360.

60. Khalak, A., and Williamson, C. H. K., 1996. Dynamics of a hydroelastic cylinder with very low mass and damping, *Journal of Fluids and Structures* 10, 455-472.

61. Khalak, A., and Williamson, C. H. K., 1997a. Fluid forces and dynamics of a hydroelastic structure with very low mass and damping, *Journal of Fluids and Structures* 11, 973-982.

62. Khalak, A., and Williamson, C. H. K., 1997b. Investigation of relative effects of mass and damping in vortex-induced vibration of a circular cylinder, *Journal of Wind Engineering and Industrial Aerodynamics* 69-71, 341-350.

63. Khalak, A., and Williamson, C. H. K., 1999. Motions, forces and mode transitions in vortex-induced vibrations at low mass-damping, *Journal of Fluids and Structures* 13, 813-851.

64. Kim E.S., Bernitsas M.M., Kumar, A.R., (2011), "Multi-Cylinder Flow Induced Motions: Enhancement by Passive Turbulence Control at 28,000<Re<120,000," Proceedings of the 30th OMAE 2011 Conf., Paper #49405, Rotterdam, The Netherlands, June 19-24, 2011; *Journal of Offshore Mechanics and Arctic Engineering, ASME Transactions*, Vol.135, No. 1, Feb. 2013.

65. Kim, S. Alam M.M., Sakamoto H., Zhou Y., 2009. Flow-induced vibrations of two circular cylinders in tandem arrangement. Part 1: Characteristics of vibration. *Journal of Wind Engineering and Industrial Aerodynamics* 97, 304–311.

66. King, R., and Johns, D. J., 1976. Wake interaction experiments with two flexible cylinders in flowing water, *Journal of Sound and Vibration* 45, 259–283.

67. Kirkgoz, M. S., Ardiclioglu, M., 1997. Velocity profiles of developing and developed open channel flow. *Journal* of *Hydraulic Engineering*, ASCE, 123, 1099-1105.

68. Kirkgoz, M.S., 1989. The turbulent velocity profiles for smooth and rough channel flow. *Journal* of *Hydraulic Engineering* 115, 1543–1561.

69. Klpfenstein R., 1998. Air velocity and flow measurement using a Pitot tube. *ISA Transactions* 37, 257-263.

70. Lam, K., Ki, J. Y., So, R.M.C., 2003a. Force coefficients and Strouhal numbers of four cylinders in cross flow, *Journal of Fluid and Structure* 18, 305-324.

71. Lam, K.M., To, A.P., 2003b. Interference of an upstream larger cylinder on the lock-in vibration of a flexibly mounted circular cylinder, *Journal of Fluid and Structure* 17, 1059-1078.

72. Laneville, A., and Brika, D., 1999, The fluid and mechanical coupling between tow circular cylinders in tandem arrangement, *Journal of Fluid and Structure* 13, 967-986.

73. Lassabatere, L., Pu, J. H., Nonakdari, Ho, Joannis C., Larrarte, F., 2013. Velocity distribution in open channel flows: Analytical approach for the outer region." *Journal* of *Hydraulic Engineering* 139, 37-43.

74. Lee, J.H., 2010. Hydrokinetic Power Harnessing Utilizing Vortex Induced Vibrations through a Virtual c-k VIVACE Model. Ph.D Thesis, Dept. of Naval Architecture & Marine Engineering, University of Michigan.

75. Lee, J.H., Bernitsas, M.M., 2011. High-damping, high-Reynolds VIV tests for energy harnessing using the VIVACE converter. *Ocean Engineering* 38, 1697-1712.

76. Lee, J.H., Xiros, N., Bernitsas, M.M., 2011. Virtual damper-spring system for VIVexperiments and hydrokinetic energy conversion. *Ocean Engineering* 38, 732-747.

77. Lee, T. and Budwig R., 1991. A study of the effect of aspect ratio on vortex shedding behind circular cylinders, *Journal of Physics of Fluids* 3,309-315.

78. Lee, T., Basu, S., 1997. Nonintrusive measurements of the boundary layer developing on a single and two circular cylinders. *Experiments in Fluids* 23, 187–192.

79. Leonard A, Roshko A. 2001. Aspects of flow induced vibration. *Journal of Fluid and Structure* 15,415-425.

80. Li, X., Dong, Z., Chen, C. (1995). Turbulent flows in smooth wall open channels with different slope. *Journal of Hydraulic Research* 33, 333–347.

81. LIGHTHILL, M. J. 1986a. An informal introduction to theoretical fluid mechanics. Oxford: Clarendon Press.

82. LIGHTHILL,M. J. 1986b. Fundamentals concerning wave loading on offshore structures. *Journal of Fluid Mechanics* 173, 667-681.

83. Lin, T. C. and SCHAAF, S. A.,1951, The effect of slip on flow near a stagnation point and in a boundary layer. NACA TN 2568.

84. Liu, X., Levitan, M., Nikitopoulos, D., 2008. Wind tunnel test for mean drag and lift coefficients on multiple circular cylinders arranged in-line *Journal of Wind Engineering and Industrial Aerodynamics* 96, 831-839.

85. Ljungkrona, L., Norberg, C., Sundén, B., 1991. Free-stream turbulence and tube spacing effects on surface pressure fluctuations for two tubes in an in-line arrangement, *Journal of Fluids and Structures* 5, 701–727.

86. Lockheed Martin - Aerospace, Defense, Security, and Advanced Technology Company, Developer of OTEC. Web. 3 May 2013. < http://www.lockheedmartin.com/us/products/otec.html>.

87. Mahir, N., Rockwell, D., 1996. Vortex formation from a forced system of two cylinders, PartI: tandem arrangement. *Journal of Fluids and Structures* 10, 473–489.

88. Mercier, J. 1973. Large amplitude oscillations of a circular cylinder in a low-speed stream. PhD thesis Stevens Institute of Technology.

89. Morison, M.P. O'Brien, J.W. Johnson, S.A. Schaaf, 1950, The force exerted by surface waves on piles Petroleum Transactions. *AIME* 189, 149–154.

90. Moriya, M., Sakamoto, H., 1986. Effect of a vibrating upstream cylinder on a stationary downstream cylinder. *ASME Journal of Fluids Engineering* 108,180–184.

91. Morsbach, M. 1967 Über die Bedingungen für eine Wirbelstraβenbildung hinter Kreiszylindern. Diss RWTH Aachen.

92. Murray, R., 2006. Review and analysis of ocean energy system development and supporting policies, International Energy Agency(IEA).

93. Nakamura, Y., Hirata, K., Kashima, K., 1994. Galloping of a circular cylinder in the presence of a splitter plate. *Journal of Fluids and Structure* 8, 355-365.

94. Nezu, I., Rodi, W., 1986. Open-channel measurements with a laser Doppler anemometer. *Journal of Hydraulic Engineering* 112, 335–355.

95. Nezu, I., and Nakagawa, H., 1993a. Turbulence in open-channel flows. IAHR-Monograph, A. A. Balkema Publishers, Rotterdam, The Netherlands.

96. Norberg, C., 2001. Flow around a circular cylinder: Aspects of fluctuating lift, *Journal of Fluids and Structures* 15, 459-469.

97. Okajima, A., 1979. Flow Around Two Tandem Circular Cylinders at Very High Reynolds Numbers, *Bulletin of JSME*, 22, 504–511.

98. Okajima, A., Sugitani, K., and Mizota, T., 1986. Flow around a circular cylinder immersed in a wake of an identical cylinder," *Trans. JSME Ser. B*, 52, 524–531.

99. Oceanlinx - Wave Energy Company, Developer of OWC, Web 3 May 2013. <http://www.oceanlinx.com>.

100. OceanPowerTechnology - Wave Energy Company, Developer of Power Buoy, Web 3 May 2013. <www.oceanpowertechnologies.com>.

101. Park H., 2012. Mapping of Passive Turbulence Control to Flow Induced Motions of Circular Cylinder. Ph.D Thesis, Dept. of Mechanical Engineering, University of Michigan.

102. Park H.R., Bernitsas M.M., Kumar, A.R., (2011), "Selective Roughness in the Boundary Layer to Suppress Flow Induced Motions of Circular Cylinder at 30,000<Re<120,000," *Proceedings of the 30th OMAE 2011 Conf.*, Paper #50302, Rotterdam, The Netherlands, June 19-24, 2011; *Journal of Offshore Mechanics and Arctic Engineering, ASME Transactions*, Vol.134, No. 4, Nov. 2012.

103. Parkinson, G.V., Sullivan, P.P., 1979. Galloping response of towers. *Journal of Industrial Aerodynamics* 4, 253-260.

104. Pelamis Wave Power - Wave Energy Company, Developer of Pelamis, Web 3 May 2013. <http://www.pelamiswave.com>.

105. Price, S.J., 1995. A review of theoretical models for fluidelastic instability of cylinder arrays in cross-flow, *J. Fluids and Structures*, 9, 463-518.

106. Raghavan K., 2007. Energy extraction from a steady flow using vortex induced vibration. Ph.D Thesis, Dept. of Naval Architecture & Marine Engineering, University of Michigan.

107. Raghavan, K., Bernitsas, M.M., 2008. Enhancement of high damping VIV through roughness distribution for energy harnessing at $8\times10^{3}<Re<1.5\times10^{5}$. 27th *International Conference on Offshore Mechanics and Arctic Engineering*, June 9-13, 2008. pp. 871-882.

108. Raghavan, K., Bernitsas, M.M., 2011. Experimental investigation of Reynolds number effect on vortex induced vibration of rigid circular cylinder on elastic supports. *Ocean Engineering* 38, 719-731.

109. Rosa D., Vieira A., 2009. Chapter4:Ocean Thermal energy converters, Fundamentals of renewable energy processes. Academic Press. pp. 139 to 152.

110. Ruscheweyh, H. P., 1983. Aeroelastic interference effects between slender structures, *Journal of Wind Engineering and Industrial Aerodynamics*14, 129–140.

111. Ruscheweyh, H. P., Dielen, B., 1992. Interference galloping-Investigations concerning the phase lag of the flow switching, *Journal of Wind Engineering and Industrial Aerodynamics* 41, 2047-2056.

112. Sarma, K. V. N., Lakshminarayana, P., and Rao, N. S. L., 1983. Velocity distribution in smooth rectangular open channels. *Journal of Hydraulic Engineering* 109, 270–289.

113. Sarpkaya, T. 1977. In-line and transverse forces on cylinders in oscillatory flow at high Reynolds numbers. *Journal of Ship Research* 21, 200-216.

114. Sarpkaya, T. 1978. Fluid forces on oscillating cylinders. ASCE *Journal of waterway, Port, Coastal, and Ocean Division* 104, 275-290.

115. Sarpkaya, T., 1986. Force on circular cylinder in viscous oscillatory flow at low Keulegan–Carpenter numbers, *Journal of Fluid Mechanics* 165, 61–71.

116. Sarpkaya, T. 1995. Hydrodynamic damping, flow-induced oscillations, and biharmonic response. *ASME Jounral of Offshore Mechanics and Arctic Engineering* 117, 232-238.

117. Sarpkaya, T., 2001. On the force decompositions of Lighthill and Morison, *Journal Fluids and Structures*, 15, 227-233.

118. Sarpkaya, T., 2004. A critical review of the intrinsic nature of vortex-induced vibrations, *Journal of Fluids and Structures* 19, 389-447.

119. Sea Generation Ltd. - Marin Current Turbine Company – Developer of SeaGen, Web 2 May 2013. <http://www.seageneration.co.uk>.

120. Shi, J., Thomas T.G., and Williams, J.J.R., 1999. Large-eddy simulation of flow in a rectangular open channel. *Journal of Hydraulic Research* 37, 345-361.

121. Steffler, P. M., Rajaratnam, N., and Peterson, A. W., 1985. LDA measurements in open channel. *Journal of Hydraulic Engineering, ASCE*, 111, 119-130.

122. Sumner, D., Price, S. J., and Paidoussis, M. P., 2000. Flow-pattern identification for two staggered circular cylinders in cross-flow, Journal of Fluid Mechanics 411, 263–303.

123. Sumner, D., Richards, M.D., Akosile, O.O., 2005. Two staggered circular cylinders of equal diameter in cross-flow, *Journal of Fluids and Structures* 20, 255–276.

124. Sumner, D., 2010. Two circular cylinders in cross-flow: A review, *Journal of Fluids and Structures* 26, 849-899.

125. Szepessy,S.,and Bearman,P.W., 1992. Aspect ratio and end plate effects on vortex shedding from a circular cylinder, *Journal of Fluid Mechanics* 234, 191-217.

126. Takahashi, M.M, 2003. Deep ocean water as our next natural resource, Terra Scientific Publishing Company, Tokyo. 13–14.

127. Tidal Electric Inc. - Tidal Power Company, Developer of Tidal Lagoons. Web 2 May 2013. <http://www.tidalelectric.com/>.

128. To, A.P., Lam, K.M., 2007. Flow-induced vibration of a flexible mounted circular cylinder in the proximity of a larger cylinder downstream, *Journal of Fluids and Structures* 23, 523-528.

129. Tracy, H. J., and Lester, C. M., 1961. Resistance coefficients and velocity distribution smooth rectangular channel, Water Supply Paper 1592-A, U.S. Geological Survey.

130. U.S. Department of Energy. Ocean Energy Technology Overview., 2009. Web. 11 April 2013. < http://www.femp.energy.gov>.

131. Vega, L., Evans, D., 1993. Operation of a small open-cycle ocean thermal Energy conversion experimental facility. library.greenocean.org.

132. Vikestad, K., 1998. Multi-frequency response of a cylinder subjected to vortex shedding and support motions, Ph.D thesis, NTNU, Norway.

133. Walker, D.T., Lyzenga, D.R., Ericson, E.A., Lund, D.E., 1996. Radar backscatter and surface roughness measurements for stationary breaking waves", *Proceeding of the Royal Society-Mathematical, Physical and Engineering Sciences Series A,* 452, 1953-1984.

134. Wang, X.W., Zhang, H.J., Zhou, Y., Tu, J.Y., 2002a. Flow visualization behind three cylinders of equal and unequal spacing. *Journal of Flow Visualization & Image Processing* 9, 139–151.

135. Werle, H., 1972. Flow past tube banks, in French, *Revue Francais de Mecanique*, Vol. 41, 7-19.

136. White, F. Viscous Fluid Flow. McGraw-Hill, 3rd edition, 2006.

137. Williamson CHK, Roshko A. 1988. Vortex formation in the wake of an oscillating cylinder. *Journal of Fluids and Structures* 2, 355–81.

138. Williamson,C.H.K., 1989. Oblique and parallel modes of vortex shedding in the wake of a circular cylinder at low Reynolds numbers, *Journal of Fluid Mechanics* 206, 579-627.

139. Williamson, C. H. K., and Govardhan, R., 2004. Vortex-induced vibrations, *Annual review of fluid mechanics 36*, 413-55.

140. Wu, J., Welch, L. W., Welsh, M. C., Sheridan, J., Walker, G. J., 1994. Spanwise wake structures of a circular cylinder and two circular cylinders in tandem, *Journal of Experimental Thermal and Fluid Science* 9, 299-308.

141. WU, J. C. 1981 The theory of aerodynamic force and moment in viscous flows. *AIAA Journal* 19, 432-441.

142. Wu W., Bernitsas M.M., Maki, K.J., 2011. RANS simulation vs. experimental measurements of flow induced motion of circular cylinder with passive turbulence Control at 30,000<Re<120,000, *Proceedings of the 30th OMAE 2011 Conf.*, Paper #50293, Rotterdam, The Netherlands, June 19-24, 2011.

143. Wu, X., Ge, F., Hong, Y., 2012. A review of recent studies on vortex-induced vibrations of long slender cylinders, *Journal of Fluids and Structures* 28, 292–308.

144. Yang, S. Q., Tan, S. K., and Lim, S. Y., 2004. Velocity distribution and dip-phenomenon in smooth uniform open channel flows. *Journal of Hydraulic Engineering* 130, 1179–1186.

145. Xu, G., Zhou, Y., 2004. Strouhal numbers in the wake of two inline cylinders. *Experiments in Fluids* 37, 248–256.

146. Zdravkovich, M. M., 1977a. Review of Flow Interference Between Two Circular Cylinders in Various Arrangements, *Journal of Fluids Engineering* 99, 618–633.

147. Zdravkovich, M.M., Pridden, D.L., 1977b. Interference between two circular cylinders; Serises of unexpected discontinuities, *Journal of Industrial Aerodynamics* 2, 255-270.

148. Zdravkovich, M. M., 1985. Flow induced oscillations of two interfering circular cylinders, *Journal of Sound and Vibration* 101, 511–521.

149. Zdravkovich, M. M., 1987. The effects of interference between circular cylinders in cross flow, *Journal of Fluids and Structures*1, 239–261.

150. Zdravkovich, M. M., 1990a. Conceptual overview of laminar and turbulent Flows past smooth and rough circular-cylinders," *Journal of Wind Engineering and Industrial Aerodynamics* 33, 53-62.

151. Zdravkovich, M.M., Medeiros, E.B., 1991. Effect of damping on interference-induced oscillations of two identical circular cylinders, *Journal of Wind Engineering and Industrial Aerodynamics* 38, 197-211.

152. Zdravkovich, M. M., 1997. Flow Around Circular Cylinders, Vol. 1, E. Achenbach, ed., Oxford University Press, Oxford, UK.

153. Zdravkovich, M. M., 2002, Flow Around Circular Cylinders, Vol. 2, E. Achenbach, ed., Oxford University Press, Oxford, UK.

154. Zippe, H. J., and Graf, W. H., 1983. Turbulent boundary-layer flow over permeable and non-permeable Tough surfaces. *Journal of Hydraulic Research*, Delft, The Netherlands, 21, 51-65.